ELUCIDATING THE WEAR MECHANISMS OF LASER SURFACE TEXTURED SURFACES

An Undergraduate Research Scholars Thesis

by

CALVIN TONG

Submitted to the Undergraduate Research Scholars program at
Texas A&M University
in partial fulfillment of the requirements for the designation as an

UNDERGRADUATE RESEARCH SCHOLAR

Approved by Research Advisor: Dr. Mathew Kuttolamadom

May 2019

Major: Mechanical Engineering

TABLE OF CONTENTS

ABSTRACT

Elucidating the Wear Mechanisms of Laser Surface Textured Surfaces

Calvin Tong
Department of Mechanical Engineering
Texas A&M University

Research Advisor: Dr. Mathew Kuttolamadom
Department of Manufacturing and Mechanical Engineering Technology
Texas A&M University

The objective of this project is to study the effects of different surface textures and patterns on the wear mechanisms involved, and the cumulative damage on these surfaces. Laser surface texturing (LST) is used to ablate metallic surfaces to impart a pattern or texture in order to improve surface tribological characteristics. The reduction in friction from LST is enabled by maintaining beneficial surface contact and lubricant adhesion/entrapment in applications such as engine bores, hard drive disks, and seals. However, the wear mechanisms of these tailored surfaces and their accumulation leading to a final wear state is not well understood. For this, a design of experiments involving numerous patterns and their variations will by created on a stainless steel surface using a high-energy laser. Their friction and wear will be characterized via standardized tests and microscopy/profilometry. It is expected that a better understanding of the wear mechanisms of LST surfaces will provide engineers an edge in designing more durable and resilient surfaces.

CHAPTER I

INTRODUCTION

Introduction

LST has a realized effect of reducing the friction as well as enhancing the boundary lubrication performance in surfaces. Micro dimples and surface grooves can be created via LST by using a controlled high energy laser. These textures help retain lubricant and allow debris to become trapped in the microcavities, thus reducing friction. [1] The surface texturing geometries that are needed to achieve these tribological benefits have been thoroughly examined. Rashwan modeled the boundary conditions of textured surfaces and related texture density to the friction coefficient, and Zhang determined that friction coefficient is dependent not only on texture geometry but also on the sliding direction and texture orientation. [1] [2] There is very little research on the types of wear mechanisms that stem from having LST treated surfaces. These mechanisms include methods such as adhesion, abrasion, corrosion, fatigue, chemical wear, etc. The industries of today need to be able to control or reduce friction and wear in surfaces in order to improve safety and operate more efficiently. [3] In the aerospace industry, the increased use of composites and aluminum has driven the need for laser-based abrading methods to make surface treatments. [4] As LST becomes more prevalent in industry, the associated change in wear properties of a LST treated surface from an untreated surface should be well documented. Having a better knowledge of wear mechanisms can help engineers choose the optimal surface texture for a particular application in order to minimize premature failure while maximizing the reduction of friction. Tribo-tests can be conducted to analyze the specific mechanisms that contribute to wear as a function of LST geometry and type. The effect of laser surface texturing

(LST) on wear and surface durability should be studied in detail in order to analyze wear mechanisms of different surface textures and geometries.

Objectives

1. Optimize laser process parameters to achieve desired surface patterns and textures
2. Formulate an experimental design that varies dimensional aspects of patterns (dimple diameter, spacing, etc.), and pattern type
3. Conduct tribological tests on wear, friction, and surface durability
4. Analyze wear mechanisms and cumulative wear states

Methodology

The goal of this research project is to elucidate the wear mechanisms which LST surfaces of different textures and geometries experience. Multiple surface textures will be created on a stainless steel surface using a high-energy fiber laser. The laser process parameters will be investigated and optimized to achieve the desired surface geometries/textures, while noting their repeatability. The geometries that are produced (based on a design of experiments) via LST will then be tested, including via standardized tribological bench tests and surface fatigue tests. Scanning Electron Microscopy along with spectroscopy and 3D surface profilometry will be utilized to analyze the wear mechanisms involved. From the data and findings of this project, designers will be able to have a better understanding of the wear mechanisms of specific LST patterns and geometries, and hence create (or choose) durable and resilient surfaces, that is best suited for a particular application.

CHAPTER II

BACKGROUND & LITERATURE REVIEW

Friction Reduction Approaches

Friction is present in every part of every mechanical system, and is a necessary component in movement and stability. By definition, it is the force that opposes sliding and slipping in an object that rolls past another surface. Although friction is a necessary component in movement and stability, excessive friction can decrease efficiency and performance in systems such as internal combustion engines and bearings. In a study published in 2012 regarding energy consumption used to overcome friction in passenger cars, it was found that 33% of energy from fuel is used to overcome friction losses, which includes engine and transmission losses. [5] This statistic presents a large area of potential improvement in terms of cost and performance in passenger cars alone. Common ways to reduce friction include polishing surfaces that come in contact, applying lubrication, decreasing the operational load on surfaces, and increasing the speed of moving components. Excessive friction over time may cause galling and damage the workpiece surface. [6] Galling occurs when lubrication breaks down between sliding surfaces, and material can severely scratch the surface and render them inoperable. Failures associated with friction can cost companies money, machine downtime, and lost productivity. It is from potential failures associated with friction such as the one described above that fuel research for improved ways to reduce friction between sliding surfaces.

One method that can be used to reduce friction between sliding contact surfaces and improve tribological performance is surface texturing. In surface texturing, shallow textures are imparted on a surface, which act as fluid reservoirs and help retain a lubrication film between the

two sliding surfaces. [7] This method is best suited for surfaces that have frequent start-stop operations, as well as planar contact surfaces. Currently, some engine piston rings use this technology in order to reduce friction by up to 25%. [8].

Texturing of Surfaces: Concept

It has been understood for many years that surface texturing can improve tribological properties in mechanical components. [9] Reducing adhesion in memory storage devices and improving efficiency in honed cylinder liners are a few of the many uses of this technology. The main principle behind surface texturing is improving the hydrodynamic boundary layer between two sliding surfaces. Additionally, surface textures act as lubrication reservoirs due to the increased surface area. Surface wetting is improved and at low load and high sliding speed conditions, where textures may act as hydrodynamic pressure areas to further reduce friction. [10] Friction reduction is centered around improving the hydrodynamic effect on a lubricated surface. Lubrication retention is also improved when certain texture patterns are used, which is a major reason for the honing pattern in cylinder liners inside internal combustion engines. Such textures can be imparted on a surface through conventional machining processes or the use of lasers. Additional methods such as vibro-rolling, various forms of etching, and abrasive jet machining have also been used to impart surface textures. [9]

In addition to the reduction of friction, surface texturing can also improve load-carrying capacity and wear resistance. Textures such as dimples or grooves act as hydrodynamic bearings in full or mixed lubrication cases and result in additional hydrodynamic pressure to increase the maximum allowable load on the surface. [11] Part longevity may also be increased through surface texturing. Surface textures help trap debris that may be dislodged from the sliding contact, thus decreasing abrasion and ploughing. [10]

Surface Texturing for Reducing Friction/Wear

Textured surfaces can be engineered to have isotropic properties, including specific real area of contact and controlled flow rate of lubrication to specifically alter the frictional performance of the surface. [11] Tests that looked at the effect of orientation and shape of each texture on friction showed that ellipses oriented perpendicular to the sliding direction had the lowest friction. [11] Therefore, texture geometry has a large effect on the friction and wear characteristics of a surface. Micro-pore patterns are becoming increasingly common in surface texturing research and are usually created using laser ablation. Etison and Burstein concluded that in mechanical seals treated with micro-pore textures, there exists an optimal selection of pore size and pore ratio (20 percent in their tests) that provides the lowest friction between two sliding surfaces. [12] In addition, in tests performed by Ronen, Etison and Kligerman, tribological characteristics were evaluated on piston rings with multiple combinations of pore depth, diameter, and number of pores. [13] The results in Figure 1 from show that friction force decreases to a certain point after which a decrease in pore depth would not yield lower values of friction force.

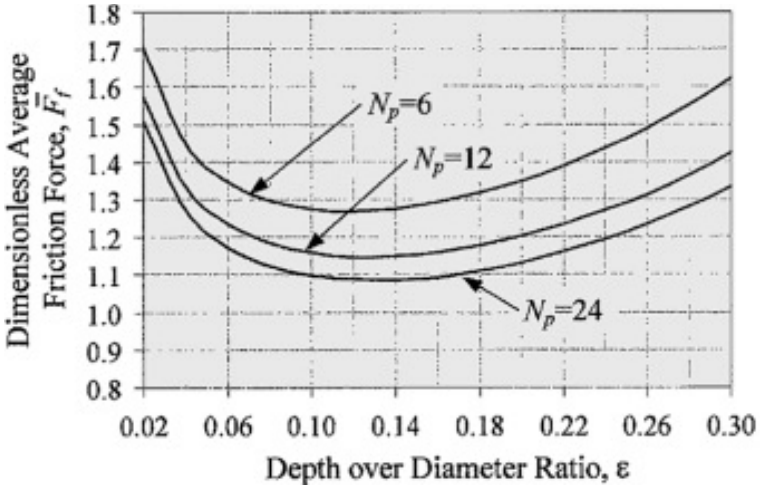

Figure 1. Dimensionless Average Friction Force v Depth/Diameter (Np= number of pores) [13]

Laser Surface Texturing for Enhancing Tribological Performance

Laser surface texturing (LST) has increasingly become more commonplace in advanced engineering materials used for applications such as automotive engines due to its flexibility and ability to meet strict surface structure design requirements. [4] Mechanical seal life can also be improved through the use of LST, with improvements of up to three times the normal life in pumps. [5] According to Rashwan, the factors that affect the resolution, ablation rate, and depth of surface textures are the wavelength of the laser, energy density, and number/duration of laser pulses, respectively. [1] These laser process parameters can be changed to create surface textures with varying friction properties. When the laser beam is focused on the workpiece, the thermal energy is absorbed and heats the surface to vaporize the material, leaving a negative texture behind. The main reason behind the use of laser ablation to impart textures is the ability to create high dimensionally accurate shapes. The primary challenge in LST is having the right laser process parameters so that the intended texture geometries can be made. Extensive research has been done on finding the optimal parameters for a given type of laser, substrate material, texture shape, and dimple density. Figure 2 shows optical micrographs of different textures made using LST on a titanium alloy disk.

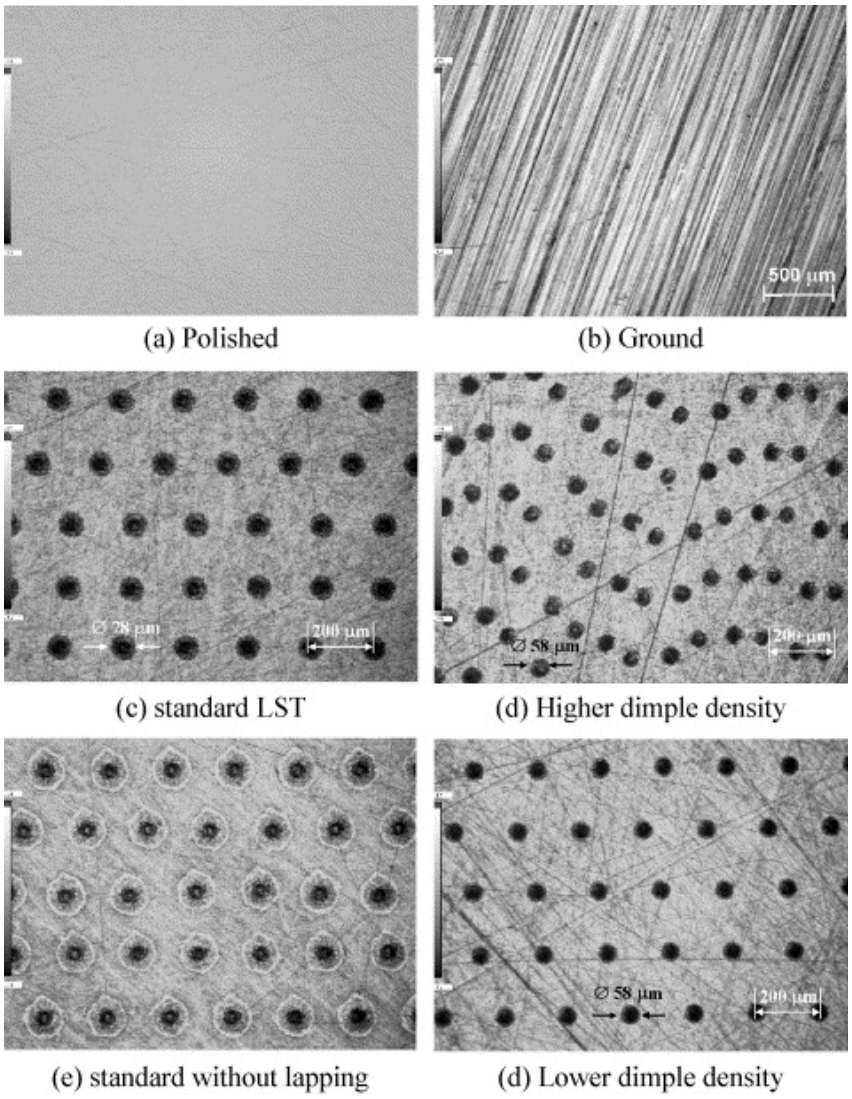

Figure 2. Optical micrograph of surface with different dimple densities [14]

Figure 3 shows an SEM image of a LST treated steel surface. Note that the hemispherical dimple contains ridges and imperfections from the laser ablation. Ablation may often eject molten material into the surroundings of the surface, which should be minimized through controlling the process parameters.

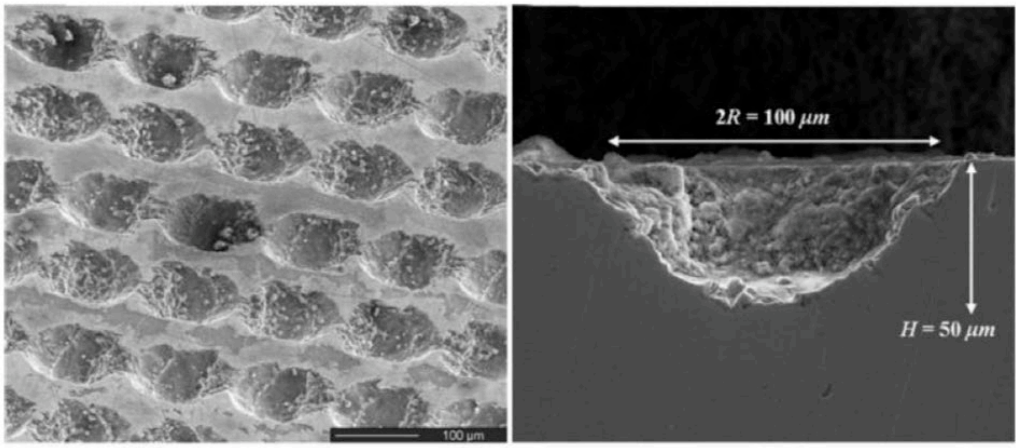

Notes: (a) 45° tilted top view; (b) perpendicular cross-section of a singular sectioned dimple: the shape could be approximated as hemi-spherical
Source: Gualtieri *et al*. (2009)

Figure 3. SEM of textured surface dimple [15]

Table 1 lists some process parameters used to create surface textures on different substrates. Laser process parameters vary depending on many factors including substrate, texture density, and type of texture. Among the most important parameters to consider are pulse width, spot duration, and scan speed.

Table 1. Process Parameters for various lasers

Laser Name	Type	Wavelength (nm)	Pulse Width (ns)	Textures Made	Source	Notes
SPI 20 W EP-S (M^2~1.1)	Fibre	1064	220		Dunn	Tested on 316 SS and low C steel
Rofin 1 kW FL010 CW	Fibre	1060				Tested on AISI D2 Tool Steel
IPG Photonics YLP 1/100/50/50	Q-Switched fibre	1064	100	Dimples, Grid, Chaotic	Demir	Max power: 50 W; 20-80 kHz PRR
YLP-1-100-20-20-RG	Fibre					Tested on Polycrystalline Diamond
Lasertec 80 Pulsed Fiber Nd:YAG laser	Fibre	1064	120	Planar, Parabolic, rotary	Sugar	Tested on 90MnCrV8 tool steel
IPG Photonics Q-Switched 50W Fibre Laser	Fibre	1064		microdimples (50 micron diameter & 2 microns depth)	Vandoni	Texturing was only applied on TiN coating (workpiece is steel)
Ti-Sapphire Laser	Fibre	800		Ripples	Bizi-Bandoki	150 fs pulses @ 5kHz with a beam diameter of 50 microns and avg power of 0.2 W on 316L SS
Nd:YAG	Fibre	1064	450	circular pores	Wan, Yi, Xiong, Dang-Sheng	Tested on T8 steel, large HAZ that requires post processing

CHAPTER III

MATERIALS & METHODS

Experimental Setup

An experimental design for laser surface texturing was first created in order to provide a means to test the friction and wear mechanisms. The laser surface texturing was done using a 200W SPI Fiber laser with a wavelength of 1098 nm and a Scanlab hurrySCAN 20 scan head with a focal length of 810 mm. The fiber laser could create a continuous or pulsed laser beam and is controlled by a laser microcontroller. The process parameters of the laser was changed by using a LasX software to modulate the laser settings and control the laser path. These settings are shown in Table 2 below.

Table 2. Laser Process Parameters

Parameter	**Range (default)**	**Description**
Spot Time	0-10,000 us	Defines how long the laser will be applied at each drill entity
Background Modulation Frequency	0-40 kHz	When enabled, this divides the main laser pulse into smaller pulses to minimize heat effects
Background Modulation Duty Cycle	0-60% (20%)	Percentage of time the laser is modulating while drilling
Jump Speed/Delay	300-15000 mm/s (2000 mm/s)	Speed at which the laser beam travels on the workspace between drill points
Position Control	1-1000 mm (10 mm)	Specifies how close the motion gets to the drill point before starting the drill

Experimental set up is shown in Figure 4 below.

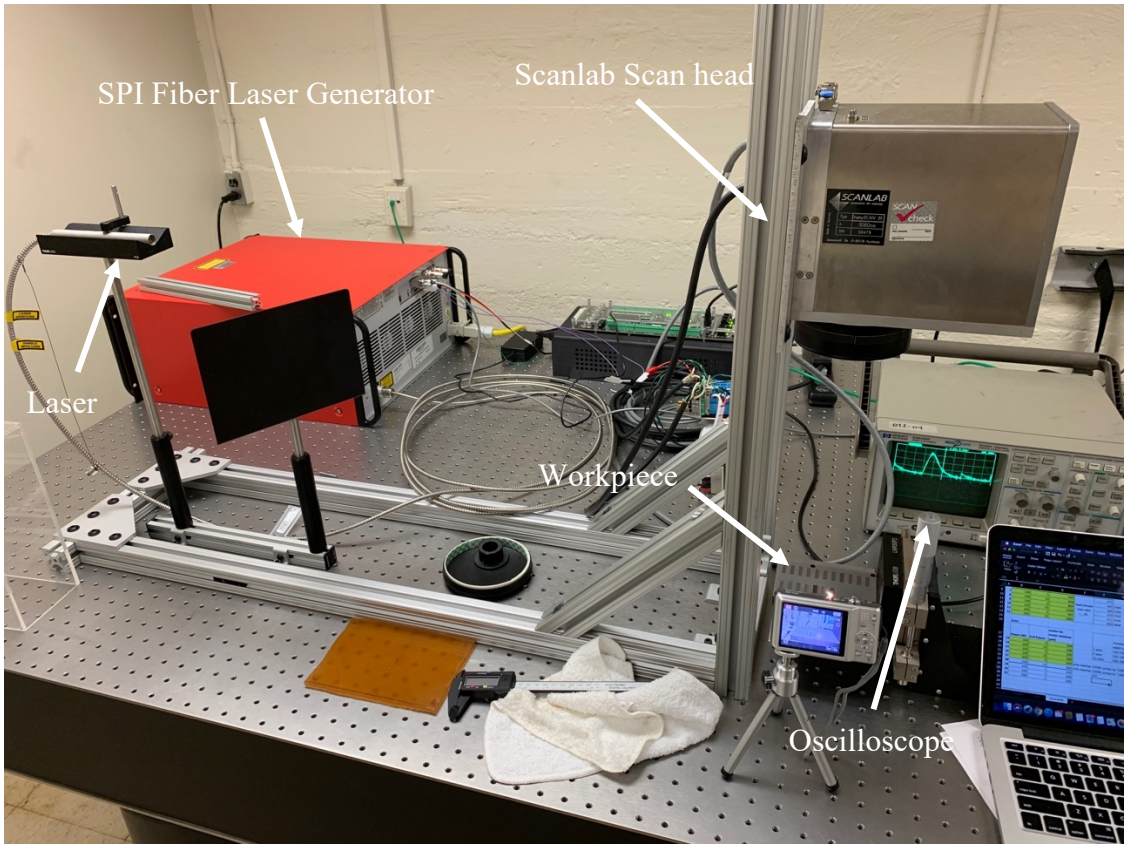

Figure 4. Laser Lab Setup

The LasX software enabled the user to define a set path for the laser to follow using a CAD-like interface. Then the texturing is ready to be made, the software sends a signal to the laser generator to emit a pulse to the scan head. The scan head has movable mirrors that adjust to create the desired geometry on the workpiece underneath.

A tribometer was used to measure the wear and friction on each textured surface. The tribometer is shown in Figure 5. The tribometer utilizes a Polycrystalline Diamond (PCD) pin to slide past the stainless steel workpiece surface and outputs a normal force to find the friction force on the surface. In addition, the sliding motion from the pin results in wear on the surface, which can be characterized through various microscopy methods including Energy-Dispersive X-Ray Spectroscopy (EDX), Scanning Electron Microscope (SEM), and other forms of surface

profile imaging. Through these instruments, specific wear mechanisms can be found for each laser surface texture.

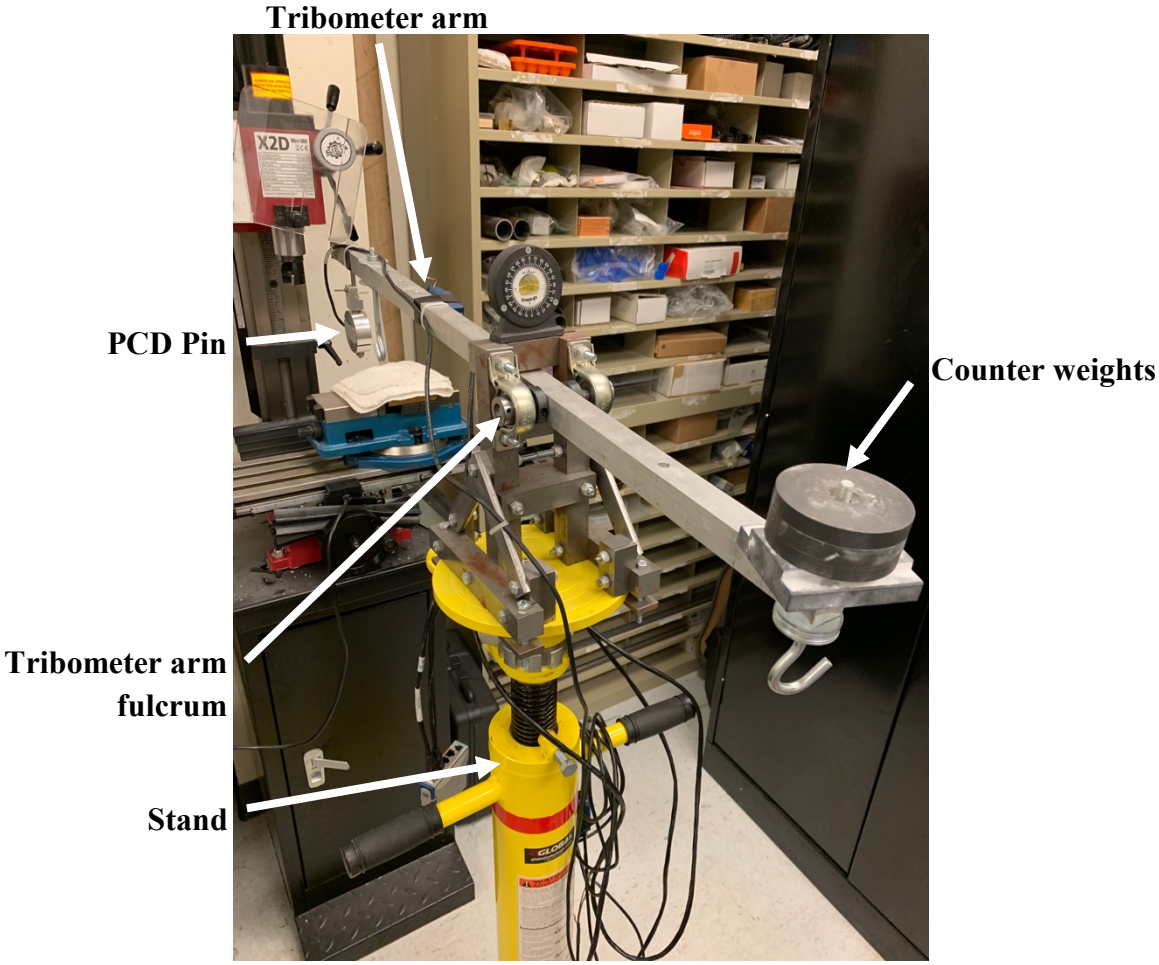

Figure 5. Tribometer Setup

Tools & Materials

All preliminary trials were conducted on a lapped 304 stainless steel flat workpiece with an average SA of 0.52 µm. Preliminary trials were done to determine laser process parameters for creating optimal surface textures. Shapes that were to be created consisted of semi-hemispherical dimples, lines, and circles. A single pulse was used to create the dimples, whereas a continuous beam was used to create both the lines and circles.

The final design of experiments was created on a 316L SS workpiece with an average SA of 1.27 um.

Design of Experiments

During preliminary trials, variables that were changed were the shape (dimples, lines, circles), laser power (100W, 150W, 200W), and number of passes (1, 5, 10, 15) and a full factorial test was performed. The number of passes represent the amount of times each individual texture was ablated with the laser in order to create the shape. In addition, for the circles, the diameters were changed (0.25 mm, 0.5 mm, 1 mm). This preliminary design of experiments is crucial in creating the optimal surface textures needed to successfully conduct the tribometer and wear tests, and is shown in Table 3.

Table 3. Preliminary Design of Experiments

Dimples		
Power (W)	**Duration (µS)**	**# of Passes**
100	10000	1
100	10000	5
100	10000	10
100	10000	15
150	10000	1
150	10000	5
150	10000	10
150	10000	15
200	10000	1
200	10000	5
200	10000	10
200	10000	15

Lines		
Power (W)	**Process Speed (mm/s)**	**# of Passes**
100	15	1
100	15	5
100	15	10
100	15	15
150	15	1
150	15	5
150	15	10
150	15	15
200	15	1
200	15	5
200	15	10
200	15	15

Table 3. Continued

Circles						
Power (W)	**Diameter (mm)**	**# of Passes**		**Power (W)**	**Diameter (mm)**	**# of Passes**
100	**0.25**	**1**		150	0.5	15
100	0.25	5		150	1	1
100	0.25	10		150	1	5
100	0.25	15		150	1	10
100	0.25	1		150	1	15
100	0.5	5		200	0.25	1
100	0.5	10		200	0.25	5
100	0.5	15		200	0.25	10
100	1	1		200	0.25	15
100	1	5		200	0.5	1
100	1	10		200	0.5	5
100	1	15		200	0.5	10
150	0.25	1		200	0.5	15
150	0.25	5		200	1	1
150	0.25	10		200	1	5
150	0.25	15		200	1	10
150	0.5	1		200	1	15

The final design of experiments was made to reflect the laser process parameters that created the best textures to test. This is reflected in Tables 4a and 4b.

Table 4a. Dimples Design of Experiments

Trial	Power (W)	# of Passes	center-to-center distance (µm)
1	100	5	750
2	100	15	750
3	150	5	750
4	150	15	750
5	200	5	750
6	200	15	750
7	100	5	660
8	100	15	828
9	150	5	864
10	150	15	1009
11	200	5	997
12	200	15	1081

Table 4b. Lines Design of Experiments

Trial	Power (W)	# of Passes	center-to-center distance (µm)
13	100	5	300
14	100	15	300
15	150	5	300
16	150	15	300
17	200	5	300
18	200	15	300
19	100	1	200
20	150	1	200
21	200	1	200

Using this design of experiments, the final stainless steel workpiece was prepped and the 21 textures were created.

CHAPTER IV

RESULTS & ANALYSES

Preliminary Test Results

Optical microscope images were taken for the textures In dimples and circles, three samples were created for each trial in order to average their depth and width and for lines, a single line was created for each trial and width and depth were found at three different spots along the line. Standard deviation within each trial was calculated to measure the variability in data for each trial. The depth and width of each texture created were found using a Zygo 3D surface profiler and an Olympus Optical microscope. Samples images from the Zygo surface profiler is found in Figures 6 and shows how the surface profile change with an increase in number of passes. Both the width and depth increase with an increase in number of passes and laser power. Perhaps most notably is that the texture appears to be more clean and less molten material is present as the number of passes increases. More of the stainless steel material is ablated with a higher number of laser pulses in a certain area. From looking at Figure 5, optical microscope images show the general shape of the textures created with the laser. At high number of passes and high laser power, there also appears to have a larger and more apparent heat affected zone around the texture. This is confirmed by looking at the zoomed in picture of the circles, where the upper left circle with 200W and 15 passes has a brownish tint around the outer diameter of the circle. This suggests a temperature of around 390 degrees celcius was achieved in the heat affected area. [16] Intergranular corrosion may be present in this area.

A Zygo surface profilometer was used to examine the geometric characteristics of the textured surfaces. The profilometer uses light rays that reflect off the surface and creates a point cloud of the geometrical features. A sample of several surface profiles that were measured are shown in Figure 6a and 6b.

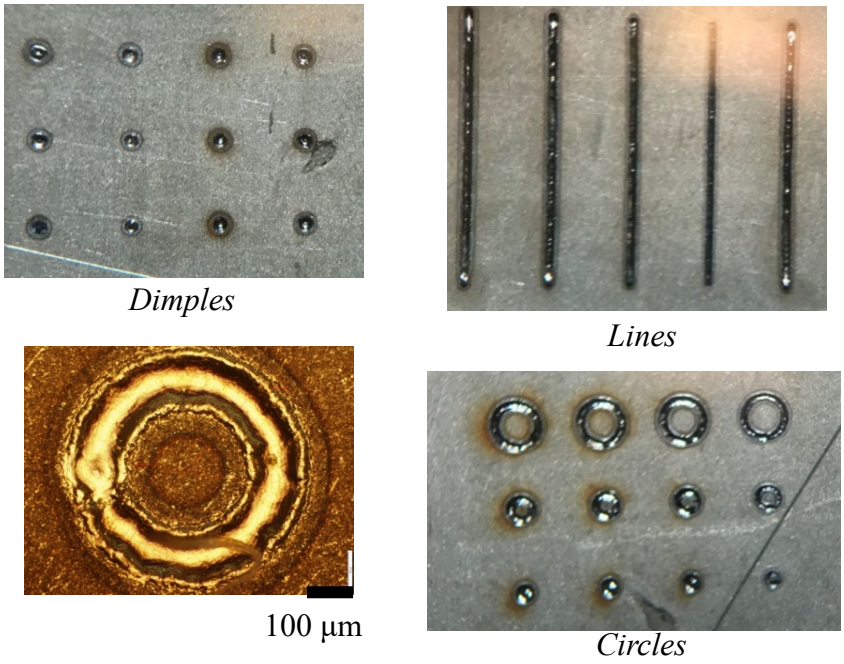

Figure 6a. Images of Preliminary Surface Textures

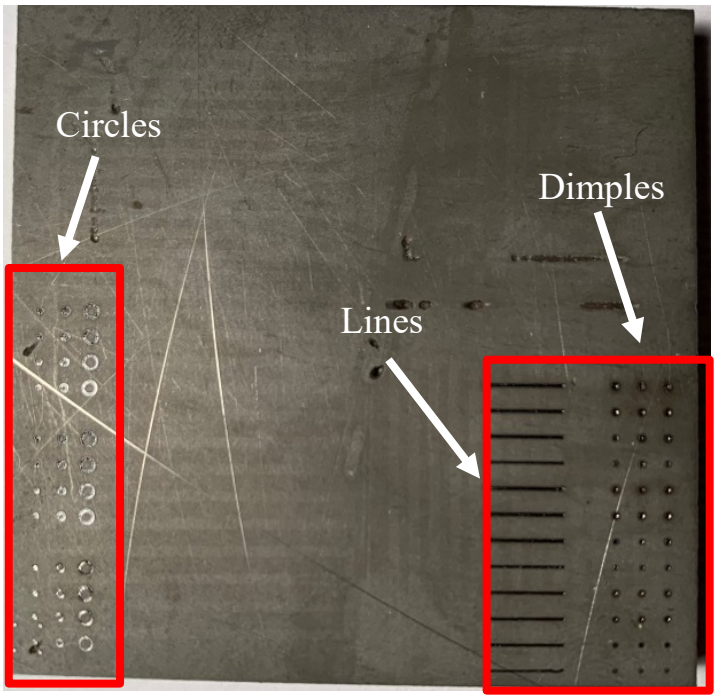

Figure 6b. Images of Preliminary Surface Textures

In Figure 7a, the dimples were made at 200W of power and varying number of passes. In the top left figure, one pass resulted in a conical indent and an average width of 360 um and depth of 16 um. There is molten material built up on the sides, as shown along the diameter of the circle. As the number of passes increase while keeping the power constant, the dimples become deeper and more circular. The variation in dimensions decrease with the number of passes, as the shape becomes more accurate and closer to the intended shape. In Figure 7b, lines are shown and the power is kept at a constant 150W while number of passes increase in a counterclockwise direction, starting from the top left. As with the dimples, a lower number of passes results in a buildup of molten material on the sides and less accurate line widths being formed. The lines become deeper and the walls become more vertical as the laser passes through more times.

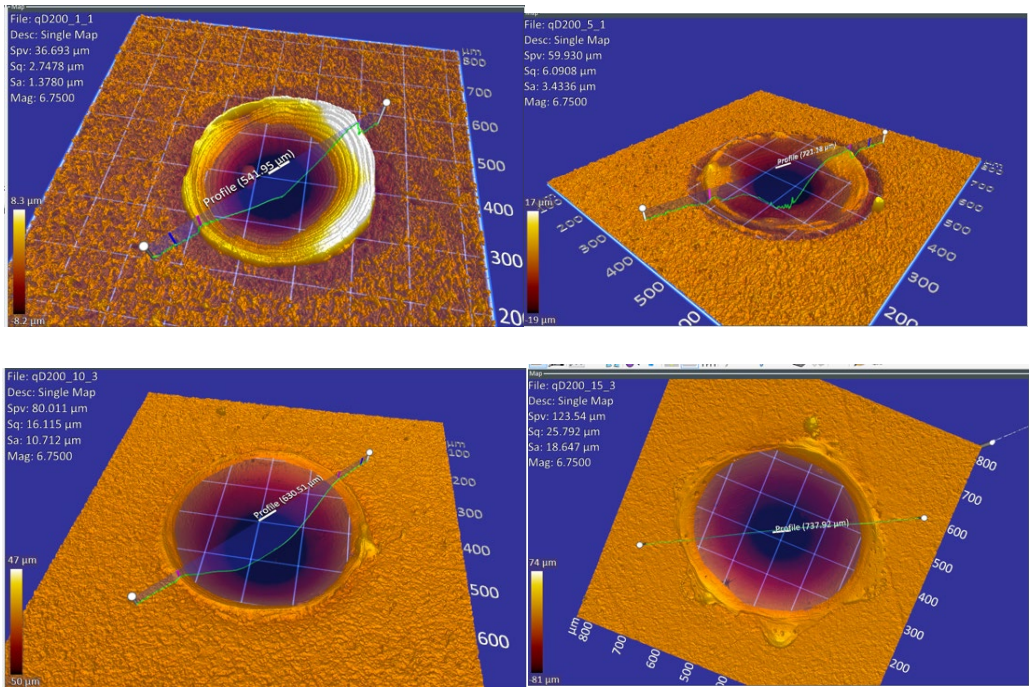

Figure 7a. Dimples at 200W and Varying # of Passes

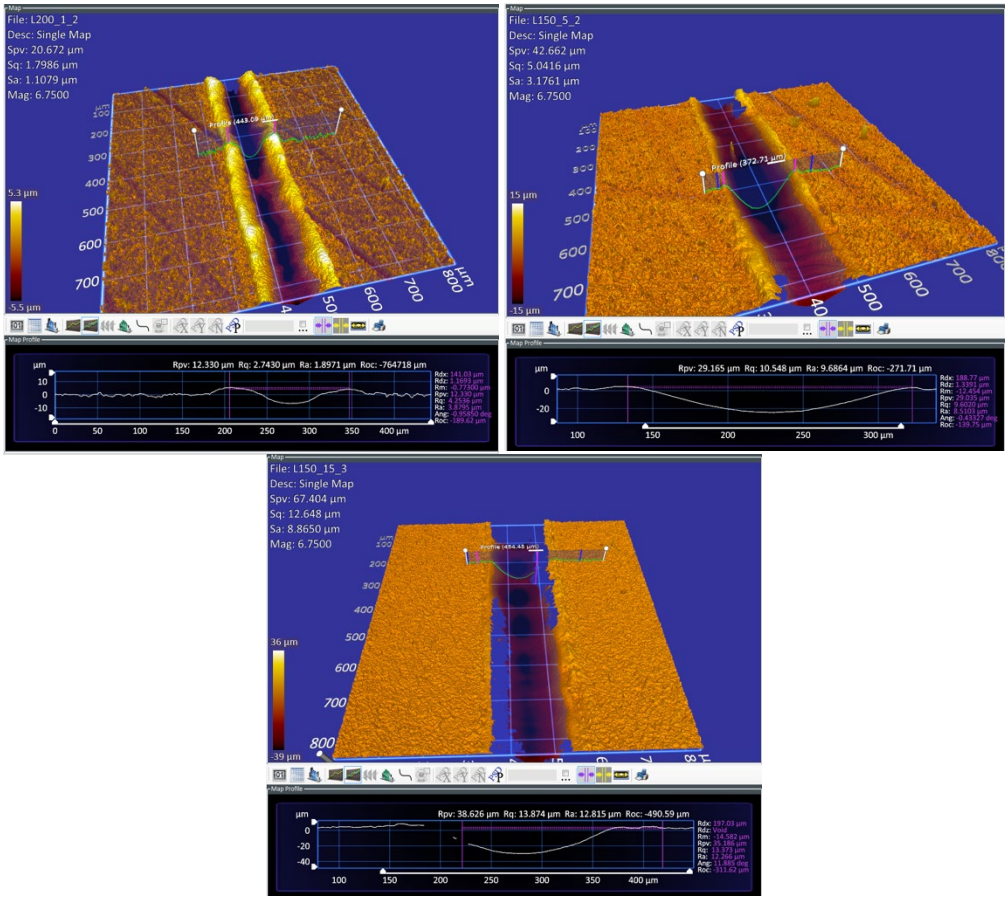

Figure 7b. Dimples at 150W and Varying # of Passes

Plots showing the dependence of depth and width on laser power and number of passes are shown in Appendix A1-A7. In addition, the raw data of width and height measurements are found in Appendix B1 and B2. Plots showing the effect of power and number of passes on the width and depth of dimple textures are highlighted in Figures 8a and 8b. In dimples, the it is shown that as the power and number of passes increase, the width and depth also increase. Error bars show the variability in each trial, and there is no real correlation between the power and number of passes on the variation in width and depth.

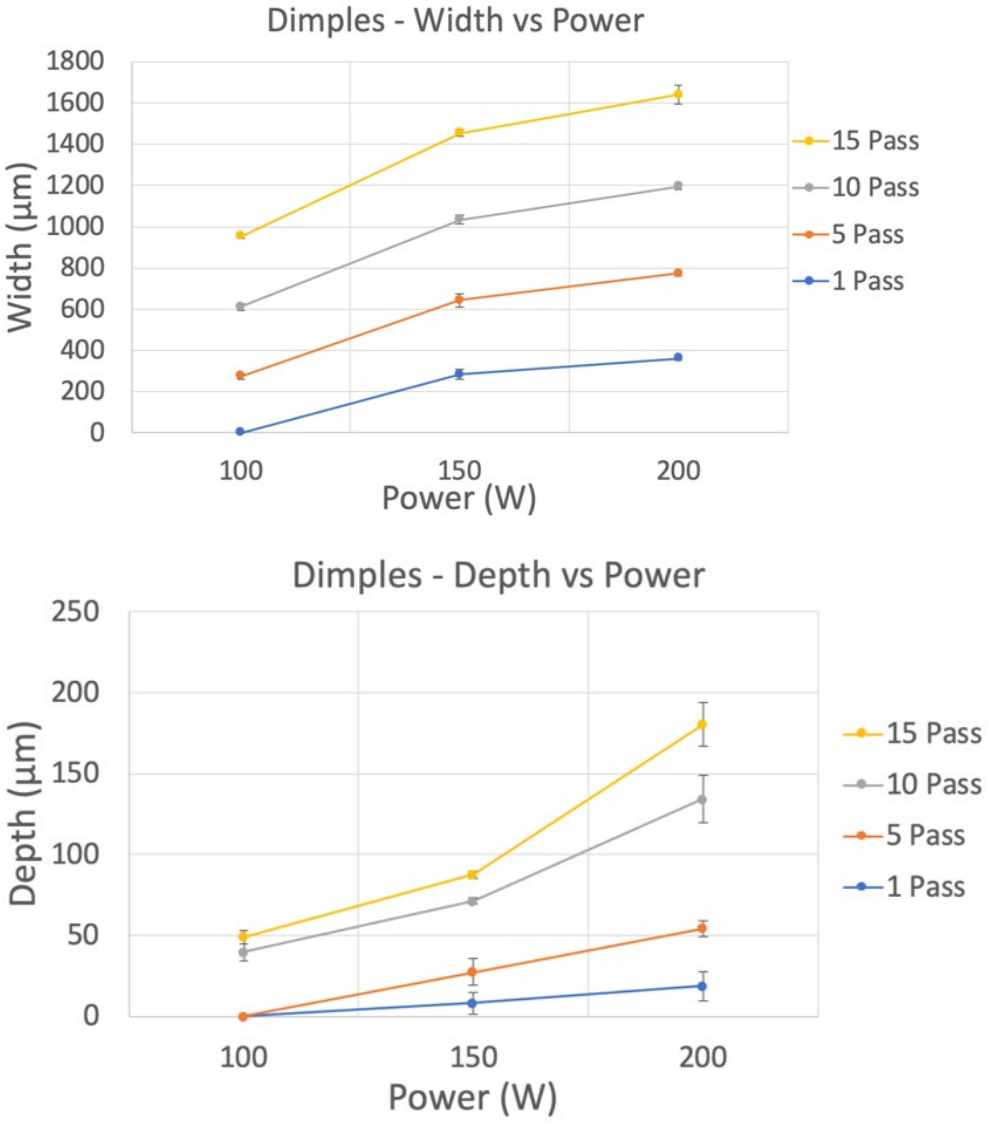

Figure 8a & 8b. Effect of Power and Number of Passes on Width and Depth of Dimples

Final Design of Experiments

It was determined that circles would not be used in the final design of experiments since the variability in each trial was too large to provide a reliable set of data each time. In addition, an increase in power does not necessarily result in an increase in diameter for circles, which is seen in both dimples and lines. Texture shapes and spacings were varied and the design of experiments can be found in Table 5a and 5b.

Table 5a. Dimples Final DOE

Texture #	**Power (W)**	**# of Passes**	**center-to-center distance (µm)**
1	100	5	750
2	100	15	750
3	150	5	750
4	150	15	750
5	200	5	750
6	200	15	750
7	100	5	660
8	100	15	828
9	150	5	864
10	150	15	1009
11	200	5	997
12	200	15	1081

Table 5b. Lines Final DOE

Texture #	Power (W)	# of Passes	center-to-center distance (µm)
13	100	5	300
14	100	15	300
15	150	5	300
16	150	15	300
17	200	5	300
18	200	15	300
19	100	1	200
20	150	1	200
21	200	1	200

Using this design of experiments, the final stainless steel workpiece was prepped and the 21 textures were created.

Dimples and lines were chosen as the shapes of choice because they had the lowest variability between each trial. The number of passes and laser power were varied, along with texture density which is measured by the center-to-center distance between each texture. Since texture density has an effect on friction, it is important to test the effect it has on wear. In trials 7-12, the variation in center-to-center distance is due to the use of a fixed area ratio (the amount of area covered by dimples) of 40%.

Final Test Results

The average SA for the final workpiece was 1.27 µm. Height and width of the textures were then tabulated and plotted in a similar manner as before. These plots can be found in Appendix A8 to A11. The trend in the dimples were generally found to be consistent with the preliminary trials. The image of the final textures are shown in Figure 9.

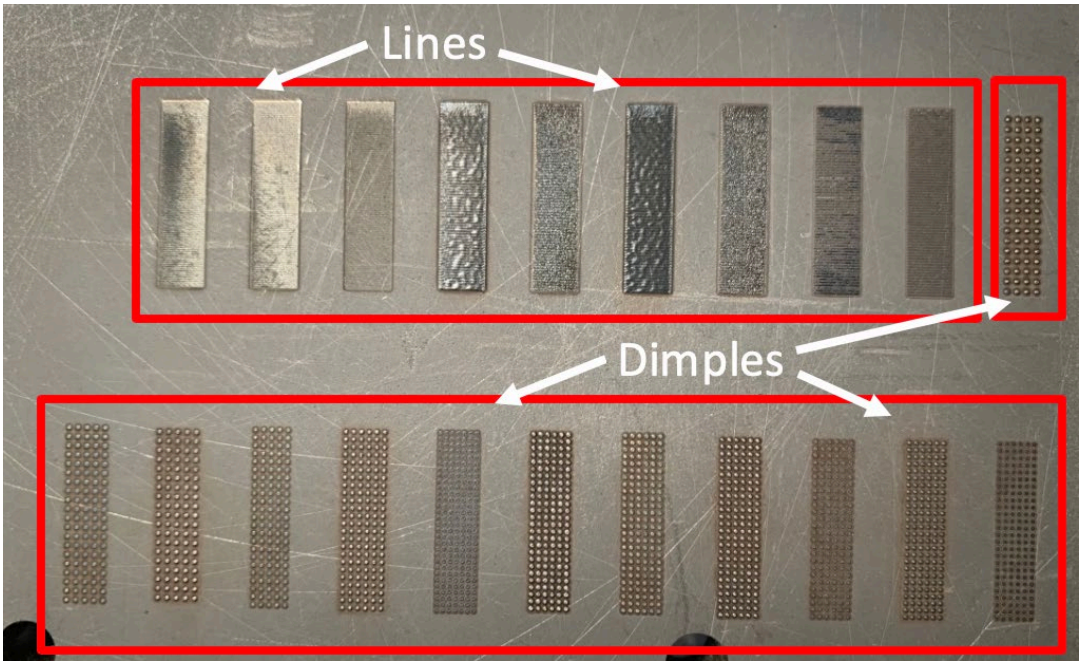

Figure 9. Final Textured Surface

Upon investigation of the textured surface under the surface profiler and optical microscope, the textures were found to be different than the ones in the preliminary trials.

In general, there are 4 main types of dimple textures that were created using the final design of experiment laser parameters. Figure 10a shows a conical protrusion with an well-defined peak, created using 100W and 15 laser passes. Figure 10b shows a smooth, short peak with a small indent in the center, likely a result of the initial laser contact with the surface. The dimple in Figure 10c has an almost perfect conical frustum with a very smooth top. This texture is particularly interesting, as the 200W and 15 laser passes has shaped the texture into a very repeatable and uniform shape.

Instead of negative textures that resulted in concave textures, the ones created were positive textures that protruded outwards. This may be due to the fact that the final workpiece used was not the same grade of stainless steel as the preliminary workpiece. The surface profile and overall texture geometry can be observed from the Zygo screenshots in Figures 10a-10d.

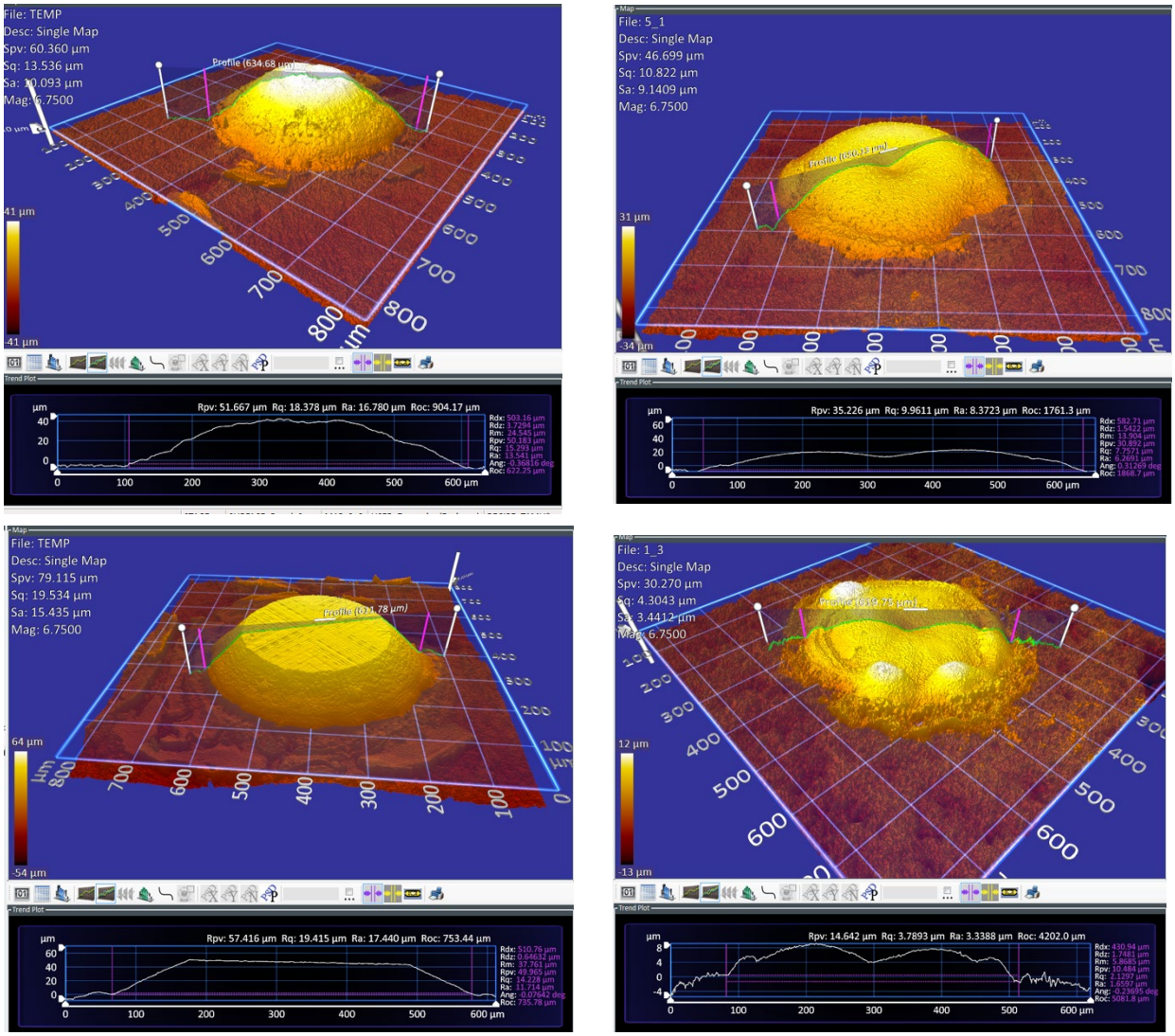

Figures 10a, 10b, 10c, 10d. (clockwise from top right) Dimple at 100W &15 Passes, Dimple at 200W & 5 Passes, Dimple at 200W & 15 Passes, Dimple at 100W & 5 Passes

Line textures did not show up well and ablated areas were indistinguishable from untextured sections of the surface, as shown in Figures 11a to 11d.

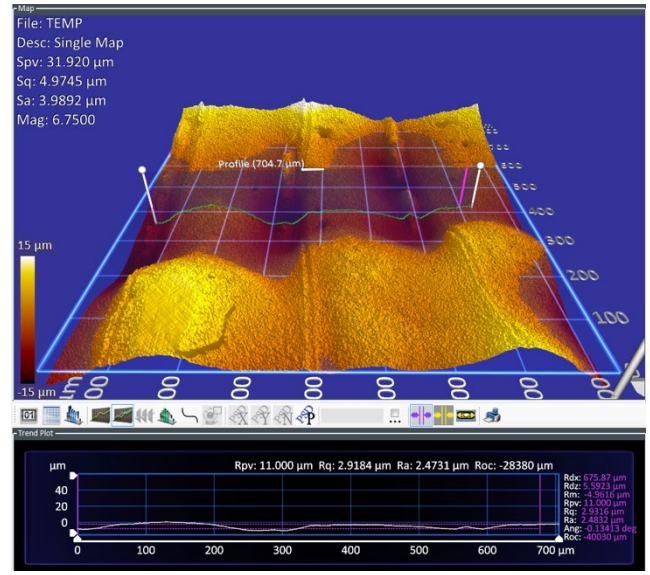

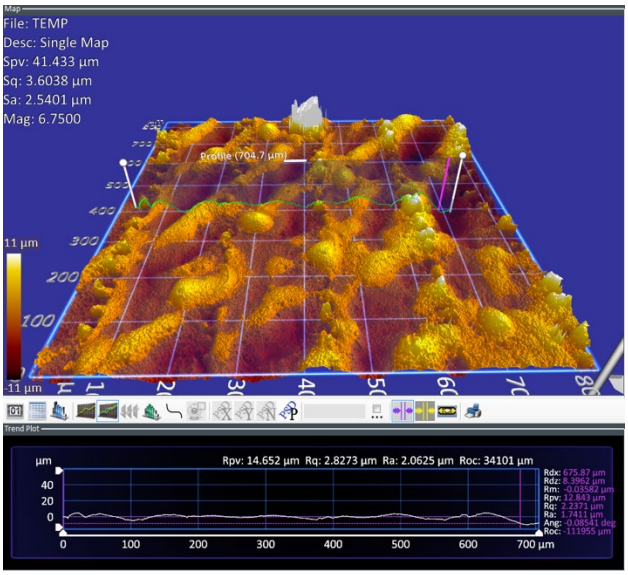

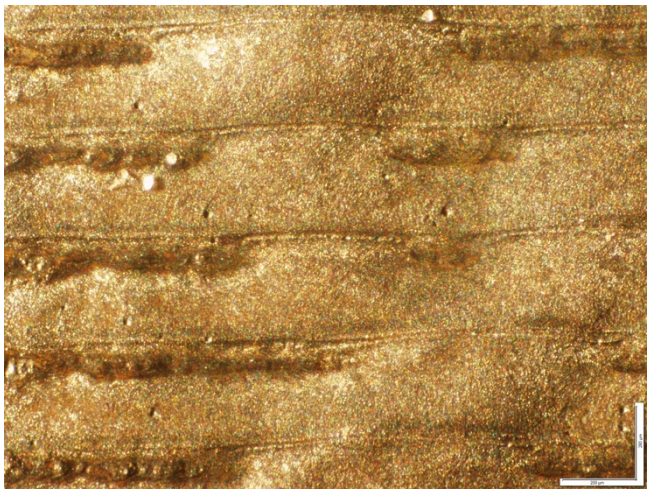

Figures 11a, 11b, 11c, 11d. (clockwise from top left) Lines at 200W & 5 Passes, Lines at 200W and 15 Passes, 5x Optical Image of Line at 200W & 5 Passes, 5x Optical Image of Line at 200W and 15 Passes

In trials with 5 laser passes (shown in Figure 11a and 11c), the textures appeared to be very faint and not representative of the textures created in preliminary trials. Trials at 15 passes did not produce textures that represented lines and were indistinguishable from the rest of the untextured surface. It is because of these reasons that geometric measurements for line textures were not possible.

Tribometer Tests

Following texturing of the final workpiece, a tribometer test was performed. The tribometer consisted of a PCD pin and two force sensors to measure the bending and compression forces on the pin as it travels over the workpiece. The compression force sensor was used to measure the normal force on the workpiece and the bending force sensor was used to measure the friction force. Using these two values, the friction coefficient could be calculated. The tribometer setup consists of a rigid arm that contains the PCD pin and all the sensors at the end. It is allowed to move up and down but is constrained in the horizontal direction. A mill is used to secure the workpiece in place and the automatic feed is turned on to ensure a consistent workpiece velocity. Both force sensors output a voltage, which is sent to a National Instruments Data Acquisition Module connected to a computer. A Labview code is used to export the voltages to an excel sheet for data manipulation. The force sensors were set to take 2500 measurements every second. The tribometer set up can be seen in Figure 12a and 12b.

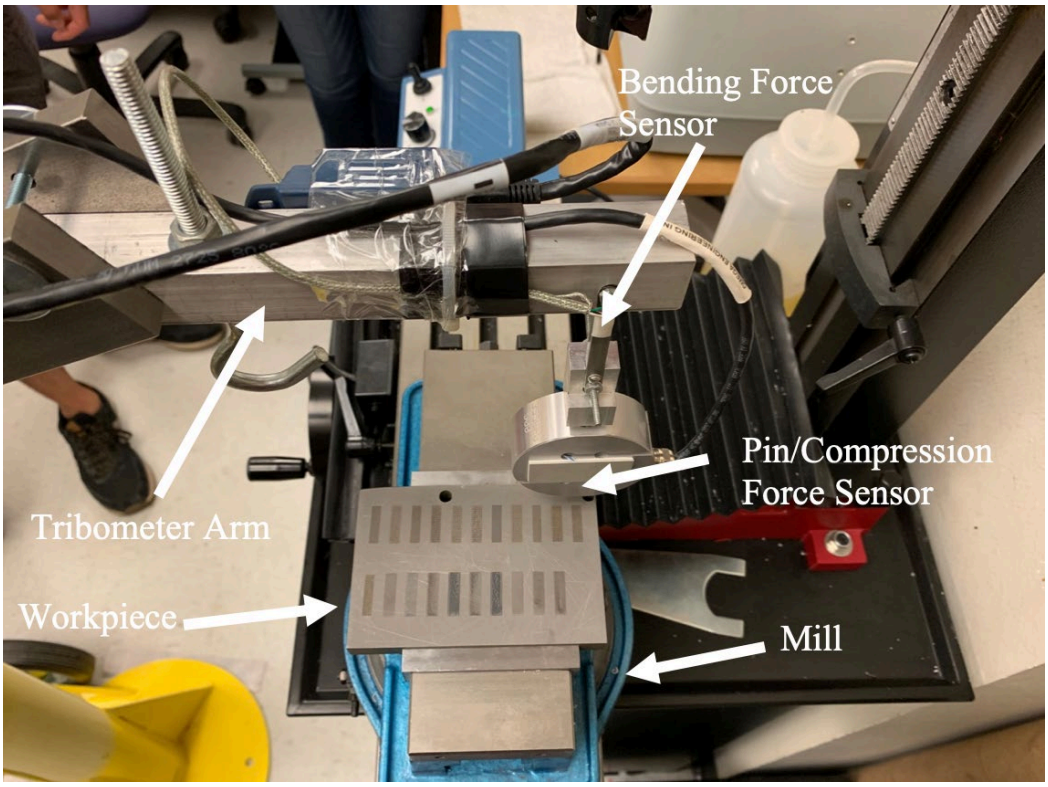

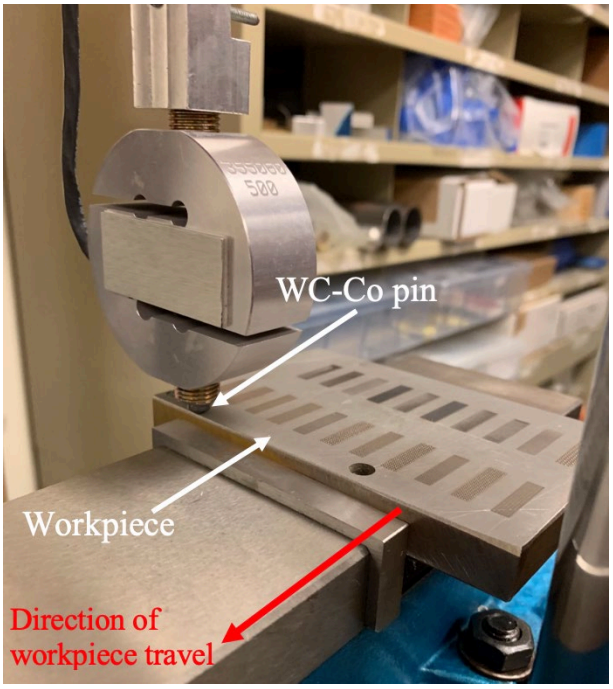

Figure 12a and 12b. Tribometer Setup

Force sensor calibration was necessary to ensure accurate force readings. To calibrate the compression force sensor, known weights from 50 g – 1500 g were placed on the end of the arm

and the corresponding voltages were recorded. A calibration curve was created using the average voltages recorded at each weight to convert voltage to force in Newtons. For the bending force sensor, a force gauge was applied to the sensor with known and constant forces from 5.5 to 23.5 N. The calibration curves are found in Appendix A Figure A12 and A13.

The experimental procedure consisted of placing the workpiece texture in line with the tribometer pin. The tribometer arm was placed orthogonal to the direction of travel of the mill. This is to ensure that the pin travels through the entire length of each texture. Figure 11b gives a view of the location of the workpiece in relation to the pin. A 1 kg weight was placed at the end of the arm to provide a known force on the pin. This also ensured that a wear mark was visible so wear mechanisms could be found using a microscope. The Labview program was first initiated, followed by the automatic feed on the mill. The program collected data until each texture was measured.

Following the tribometer tests, plots of output voltage from the bending and compression force sensors were created. Figure 13 shows one of the plots, whereby from looking at the bending beam plot it is apparent that there are two sections where the tribometer passed over textures 1 and 12 (around 8000 samples and 15500 samples). The complete raw data plots are found in Appendix A14.

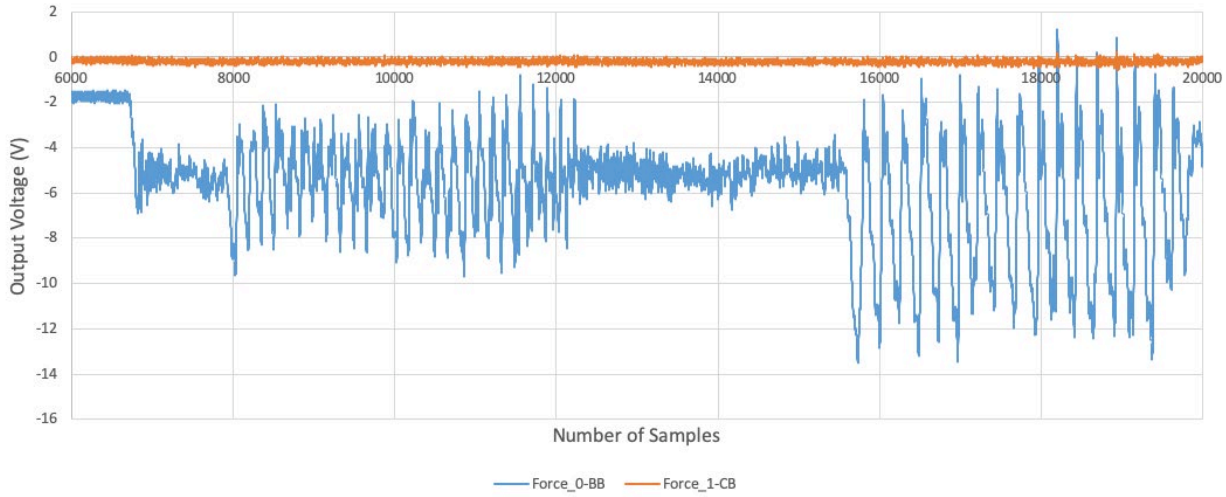

Figure 13. Raw Data of Force Sensor Output Voltage for Textures 1 & 12

The average voltages in these sections were used to find the friction force, normal force, and friction coefficient for each sample, which is tabulated in Table 6 below.

Table 6. Tribometer Test Results

Texture	Power (W)	# of Passes	Friction Force (N)	Friction Force st. dev (N)	Normal Force (N)	Normal Force st. dev (N)	Friction Coefficient
1	100	5	1.788	-0.260	9.940	5.381	0.180
2	100	15	3.163	0.201	10.050	4.977	0.315
3	150	5	1.819	-1.113	10.486	5.620	0.173
4	150	15	2.494	0.137	10.362	5.163	0.241
5	200	5	2.733	-0.301	10.325	5.291	0.265
6	200	15	2.605	0.194	10.066	5.163	0.259
7	100	5	1.782	-0.376	9.844	5.393	0.181
8	100	15	2.737	-0.236	9.968	5.343	0.275
9	150	5	2.105	-0.381	10.556	5.403	0.199
10	150	15	2.316	0.009	10.529	5.350	0.220
11	200	5	2.320	-0.379	10.541	5.394	0.220
12	200	15	2.610	0.536	10.208	5.117	0.256

CHAPTER V

CONCLUSIONS & DISCUSSIONS

Although the final design of experiments did not yield the results that were expected based on the preliminary trial, important info can still be extrapolated from tribometer tests in future work. It is known that in both preliminary and final trials for LST, the dimensions of the textures increase with an increase in laser power and number of passes. There is less slag and molten material with an increase in number of passes. With the final design of experiments, the dimples changed shape from a circular molten mound at low power and low number of passes to a conical frustum-like shape at high power and high number of passes.

The difference in material (304 SS in preliminary trials vs 316L SS in the final trials) contributed to the difference in texture geometries created. The effect of the fiber laser on a surface depends on the wavelengths of the laser beam that is absorbed by the surface. Since 316L stainless steel contains more nickel than 304 SS, this difference in chemical composition most likely contributed to the difference in textures created.

Plots showing the relationship between the friction coefficient of each texture and its process parameter and geometry were created. Figure 14 shows the relationship between the friction coefficient and laser power. It can be seen that generally friction coefficient of each texture is the greatest at 100W of power. The 15 pass textures had higher friction coefficients than the 5 pass textures, which may be a result of more buildup of material at a 15 passes.

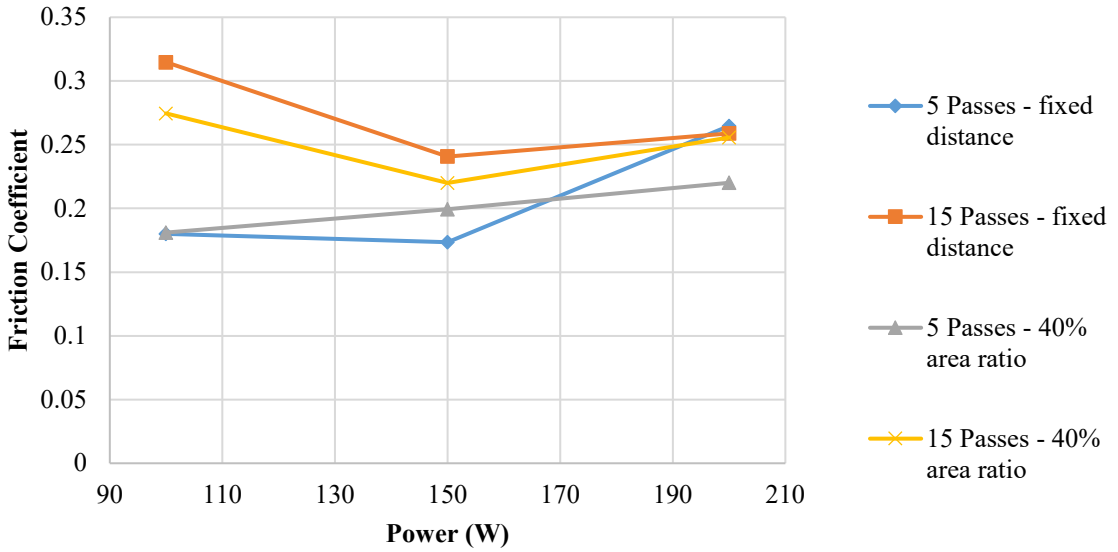

Figure 14. Friction Coefficient v Laser Power

In addition, friction coefficient was plotted against the surface roughness, or SA of each texture, as shown in Figure 15. The friction coefficient tends to increase with a corresponding increase in SA. Rougher surfaces tend to have higher friction, as expected. At an SA of approximately 10 um, there appears to be a spike in friction coefficient.

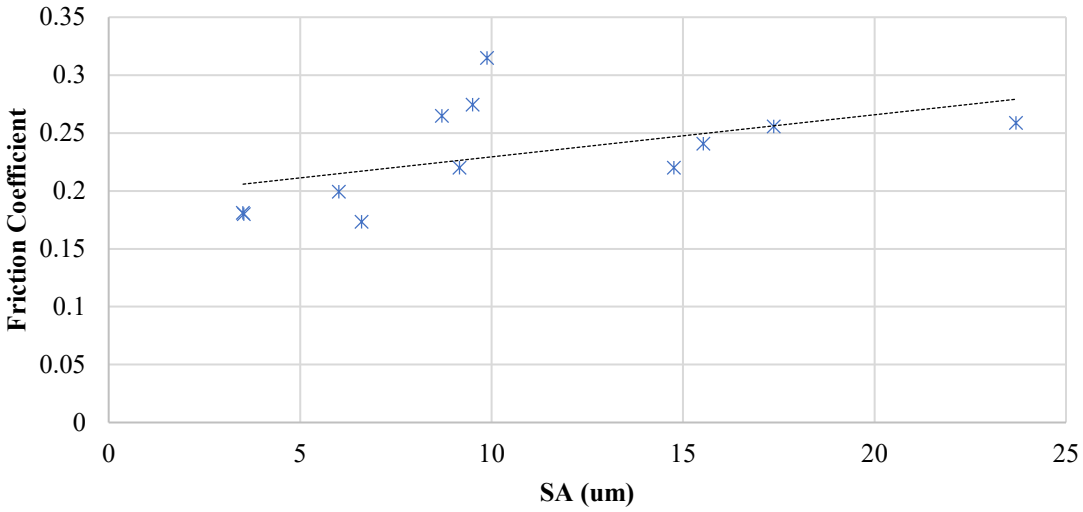

Figure 15. Friction Coefficient v Surface Roughness

Two plots, Figures 16 and 17 show the dependency of friction coefficient on the geometry of each texture. The untextured surface of the workpiece had an average friction coefficient of 0.131. The diameter and height values shown represent an average of 3 measurements on each texture. In the relationship between friction coefficient and the diameter of the texture, there appears to be a positive correlation between the two variables. Larger diameter textures tended to have higher friction coefficients, save for a few outliers at 477 um and 482 um, which exhibited higher friction coefficients than expected. In general, larger diameter and taller textures have higher friction coefficients.

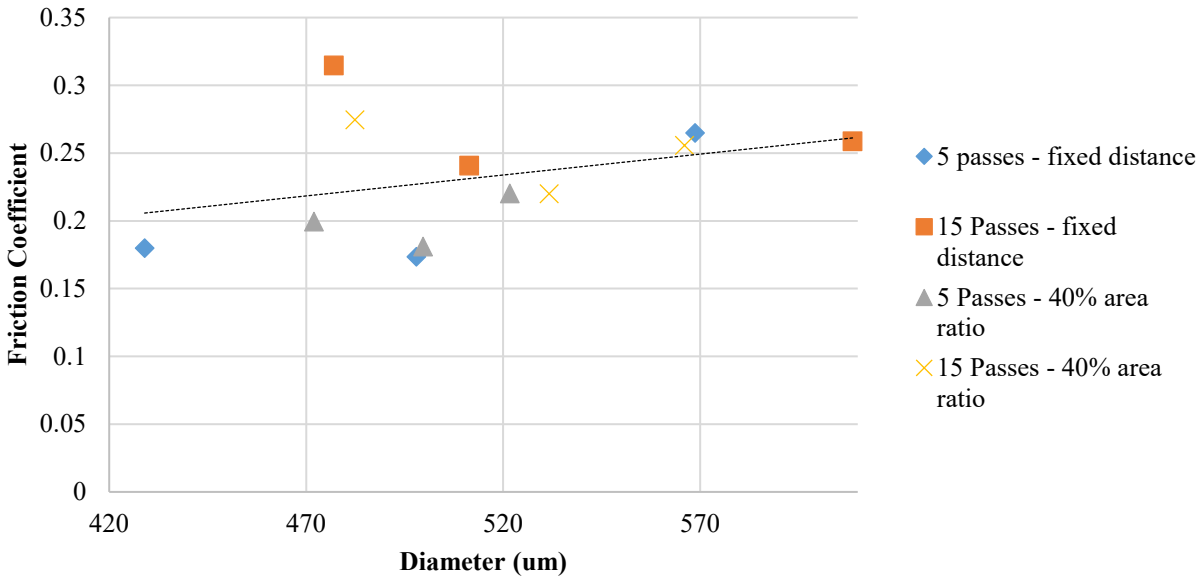

Figure 16. Friction Coefficient v Diameter

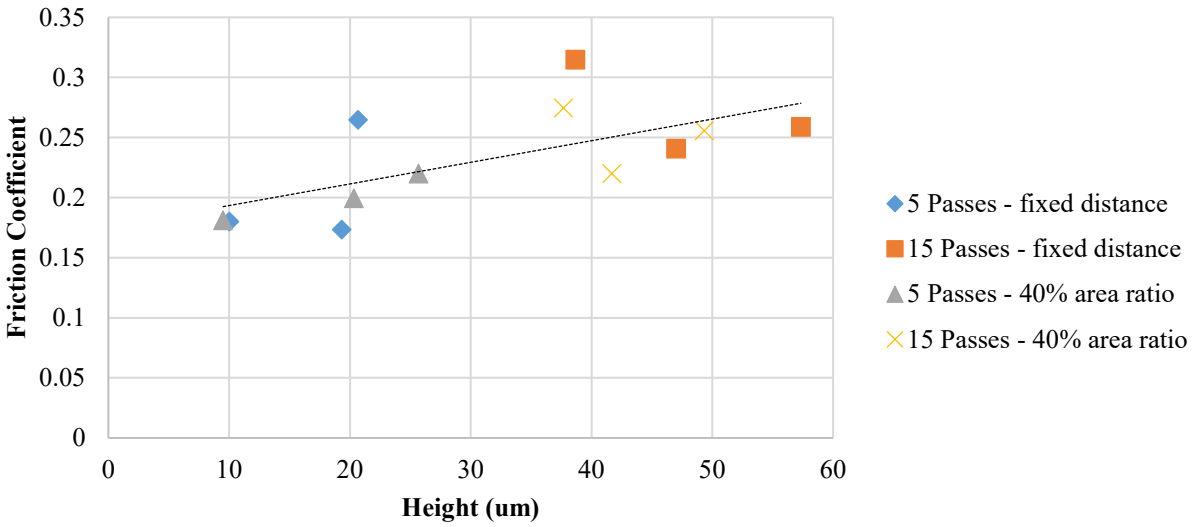

Figure 17. Friction Coefficient v Height

Optical microscope images captured wear effects of the tribometer ball on the surface of the workpiece. These images are shown in Figure 18. From the images, the main form of wear consists of abrasion, whereby there exists visible wear marks in the direction of the pin travel. The wear marks span one dimple in some cases, and two dimples in other cases. The contact position of the pin on the texture as it slides across the workpiece can affect the friction characteristics. In some tests, the pin was sliding across one dimple, and in other tests, the pin slided across multiple dimples, which would increase the measured friction force. Also notable is the fact that the pin only made contact with the dimples itself and not the untextured flat surface of the workpiece. There is no visible evidence of wear on the flat surface. Future analysis including energy-dispersive X-ray spectroscopy can be used to look for evidence of other forms of wear on the surface of the laser textured surface.

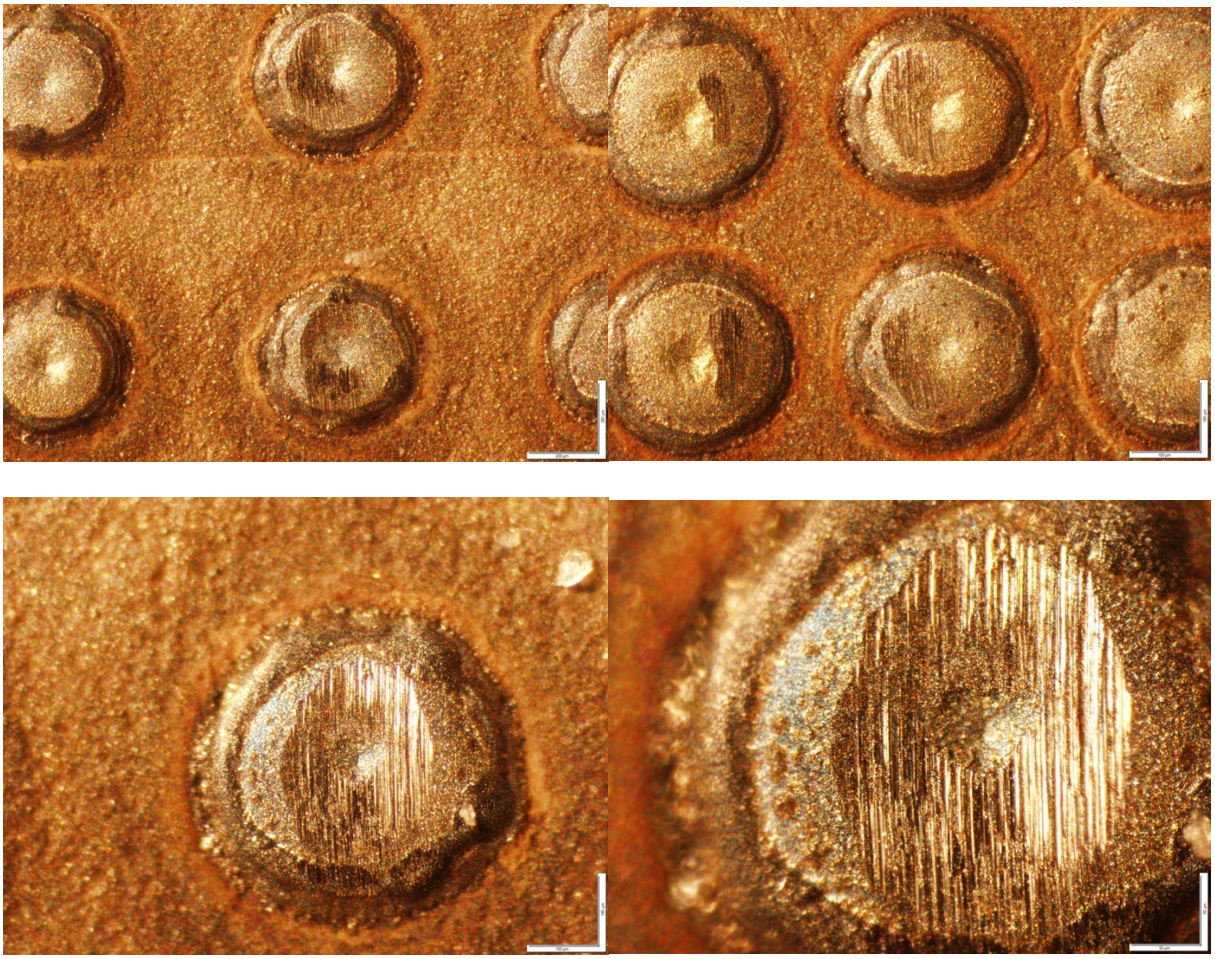

Figure 18. Optical Microscope Images of Wear Effects

REFERENCES

[1] Rashwan, O., "Micro Surface Texturing for Friction Control" (2013). *Electronic Theses and Dissertations*. 4869.

[2] Zhang, S., Zeng, X., Igartua, A., Rodriguez- Vidal, E., van der Heide, E. (2017*). Texture Design for Reducing Tactile Friction Independent of Sliding Orientation on Stainless Steel Sheet.*

[3] Pettersson, U. 2005. *Surfaces Designed for High and Low Friction*. (Ytor utformade för hög och låg friction). Acta Universitatis Upsaleiensis. Digital Comprehensive Summaries of Uppsala Dissertations from the Faculty of Science and Technology 63. 43 pp. Uppsala. USBN 91-554-6278-2.

[4] See, T.L. (2015). *Laser Surface Texturing – Fundamental Study and Applications*. (Doctorate Thesis).

[5] Holmberg, K., Andersson, P., & Erdemir, A. (2011, December 06). Global energy consumption due to friction in passenger cars.

[6] Heide, E. V., & Schipper, D. (2003). Galling initiation due to frictional heating. *Wear,254*(11), 1127-1133. doi:10.1016/s0043-1648(03)00324-7

[7] Wakuda, M., Yamauchi, Y., Kanzaki, S., & Yasuda, Y. (2003). Effect of surface texturing on friction reduction between ceramic and steel materials under lubricated sliding contact. *Wear,254*(3-4), 356-363. doi:10.1016/s0043-1648(03)00004-8

[8] Wakuda, M., Yamauchi, Y., Kanzaki, S., & Yasuda, Y. (2003). Effect of surface texturing on friction reduction between ceramic and steel materials under lubricated sliding contact. *Wear,254*(3-4), 356-363. doi:10.1016/s0043-1648(03)00004-8

[9] Etsion, I. (2005). State of the Art in Laser Surface Texturing. *Journal of Tribology,127*(1). doi:10.1115/esda2004-58058

[10] Andersson, P., Koskinen, J., Varjus, S., Gerbig, Y., Haefke, H., Georgiou, S., . . . Buss, W. (2007). Microlubrication effect by laser-textured steel surfaces. *Wear,262*(3-4), 369-379. doi:10.1016/j.wear.2006.06.003

[11] Yu, H., Wang, X., & Zhou, F. (2010). Geometric Shape Effects of Surface Texture on the Generation of Hydrodynamic Pressure Between Conformal Contacting Surfaces. *Tribology Letters,37*(2), 123-130. doi:10.1007/s11249-009-9497-4

[12] Etsion, I., & Burstein, L. (1996). A Model for Mechanical Seals with Regular Microsurface Structure. *Tribology Transactions,39*(3), 677-683. doi:10.1080/10402009608983582

[13] Ronen, A., Etsion, I., & Kligerman, Y. (2001). Friction-Reducing Surface-Texturing in Reciprocating Automotive Components. *Tribology Transactions,44*(3), 359-366. doi:10.1080/10402000108982468

[14] Kovalchenko, A., Ajayi, O., Erdemir, A., Fenske, G., & Etsion, I. (2005). The effect of laser surface texturing on transitions in lubrication regimes during unidirectional sliding contact. *Tribology International,38*(3), 219-225. doi:10.1016/j.triboint.2004.08.004

[15] Ryk, G., & Etsion, I. (2006). Testing piston rings with partial laser surface texturing for friction reduction. *Wear,261*(7-8), 792-796. doi:10.1016/j.wear.2006.01.031

[16] Engineer, A. B. (2016, June 28). All you need to know about the heat-affected zone. Retrieved from https://www.thefabricator.com/article/shopmanagement/all-you-need-to-know-about-the-heat-affected-zone

APPENDIX A

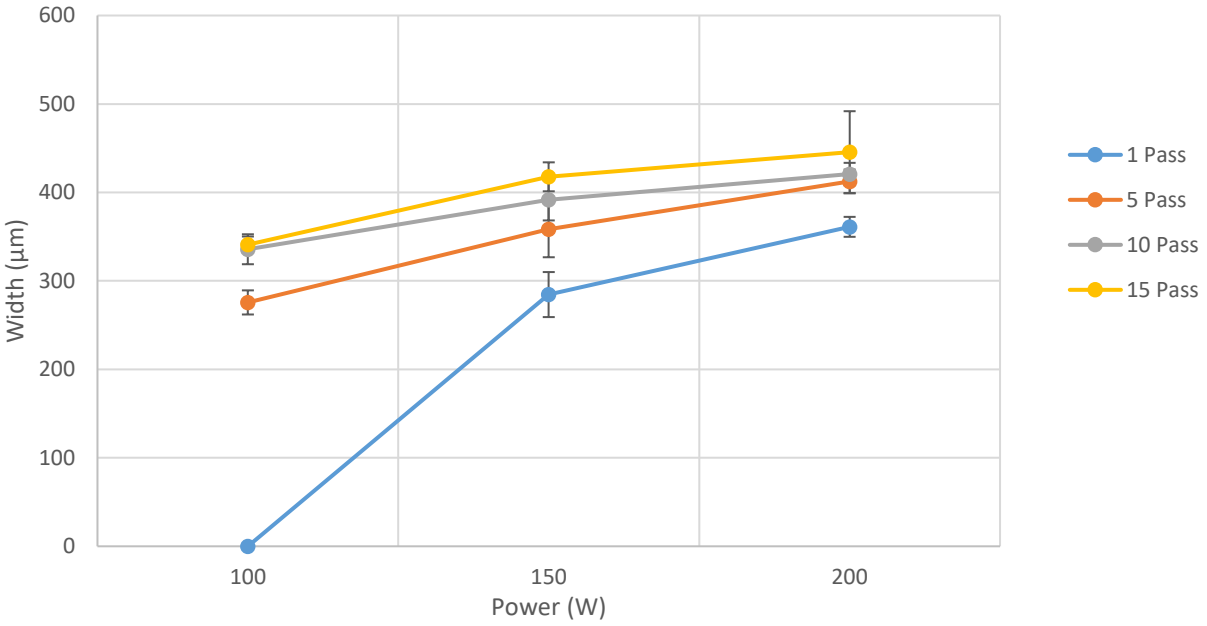

Figure A1. Dimples – Width vs Power

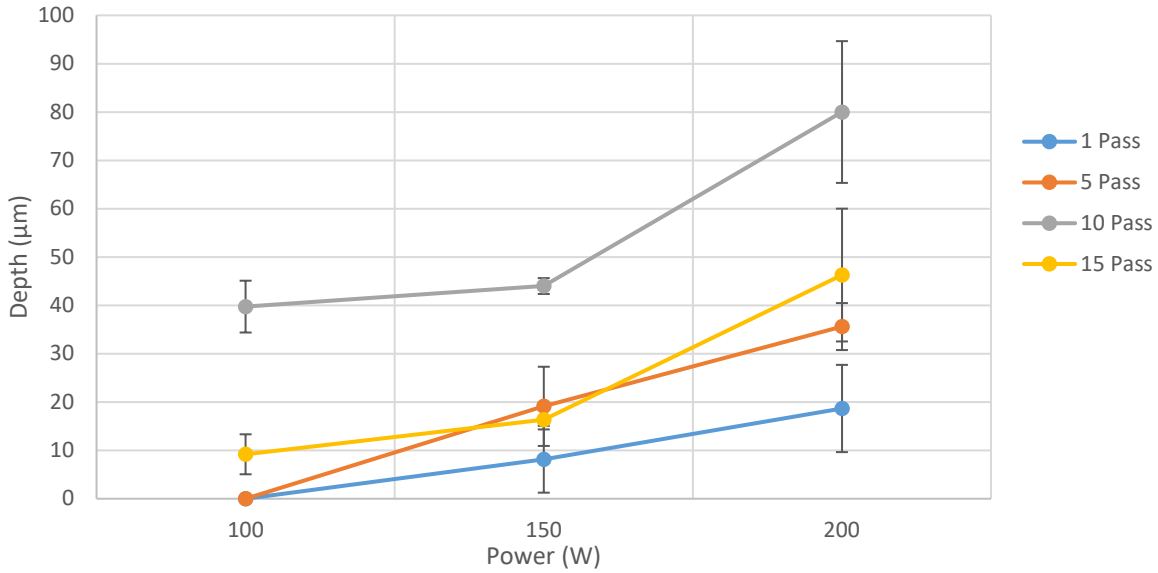

Figure A2. Dimples - Depth vs Power

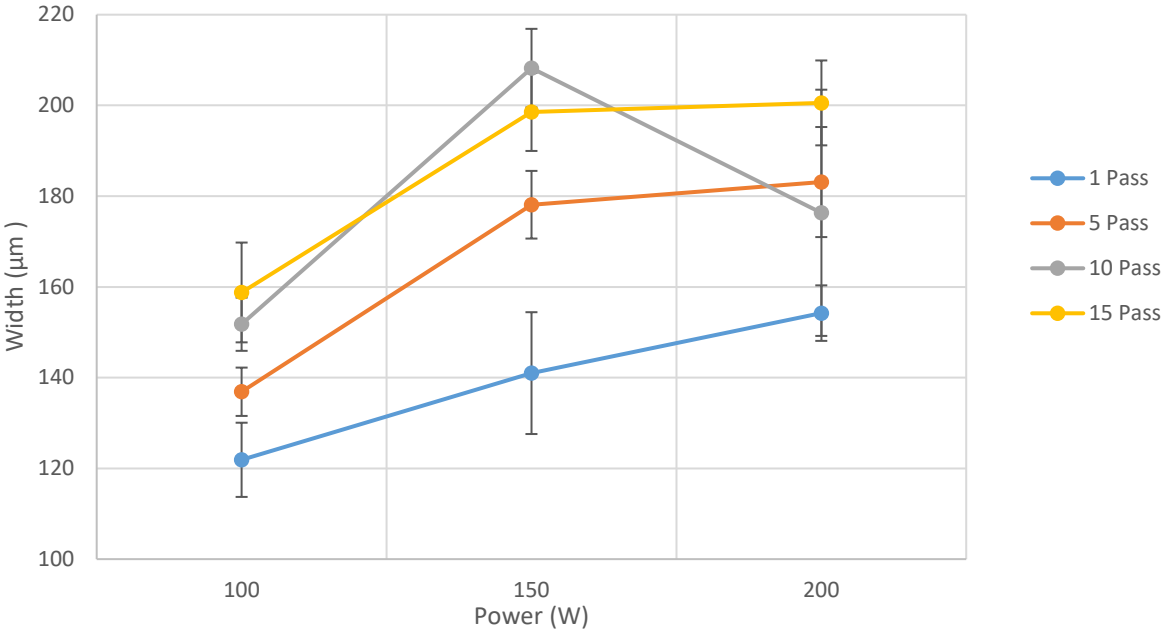

Figure A3. Lines – Width vs Power

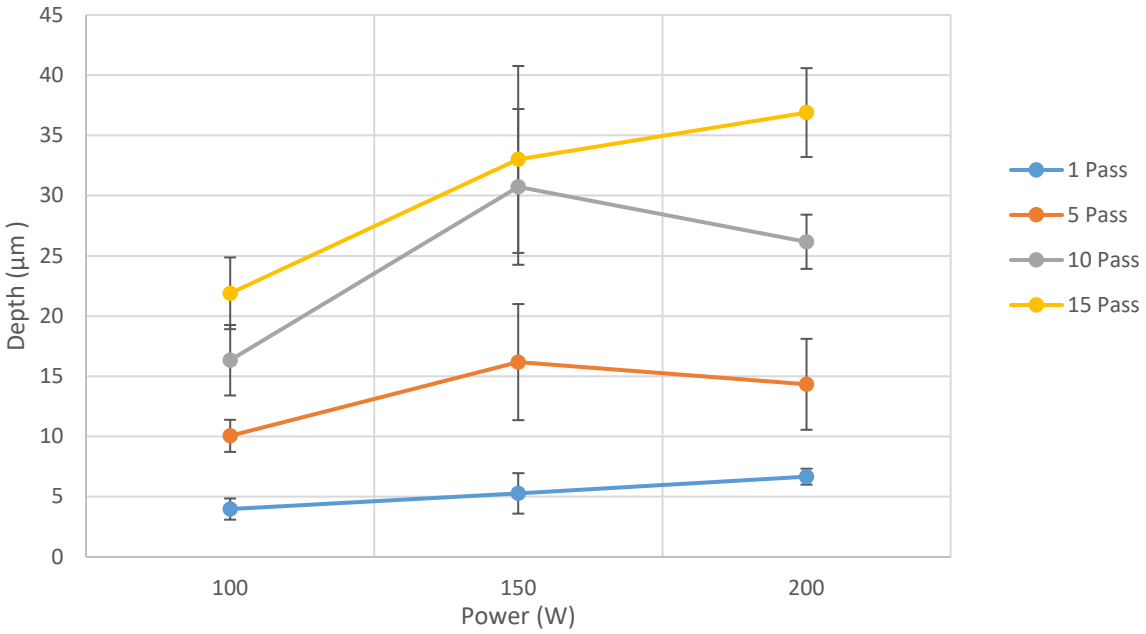

Figure A4. Depth vs Power

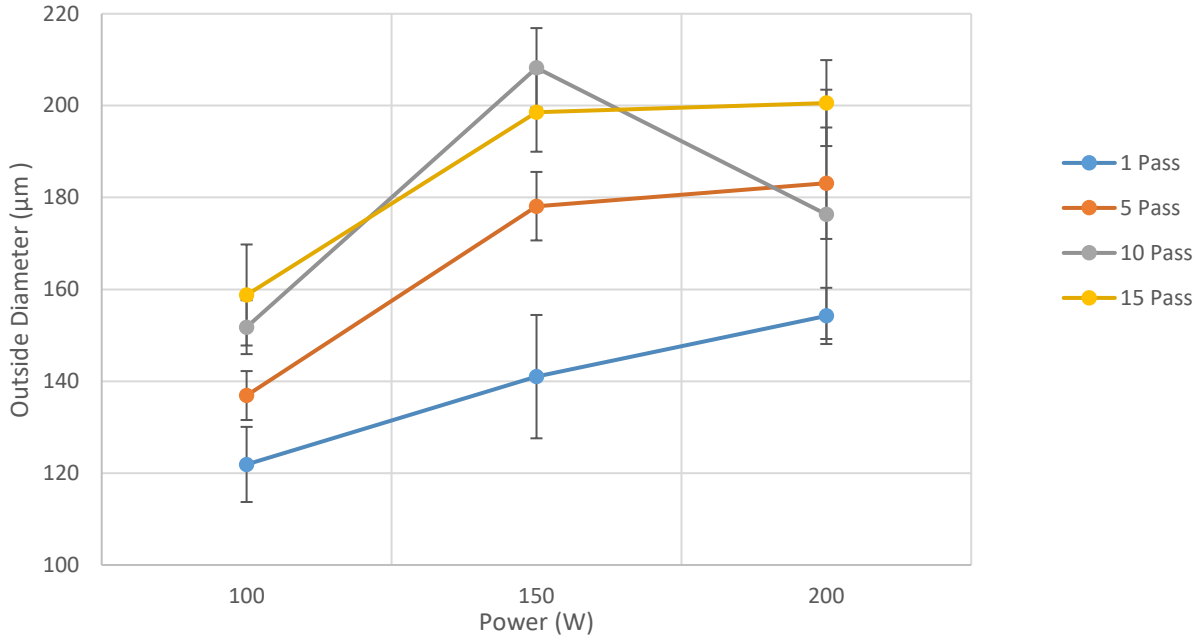

Figure A5. Circles - 0.25 mm OD vs Power

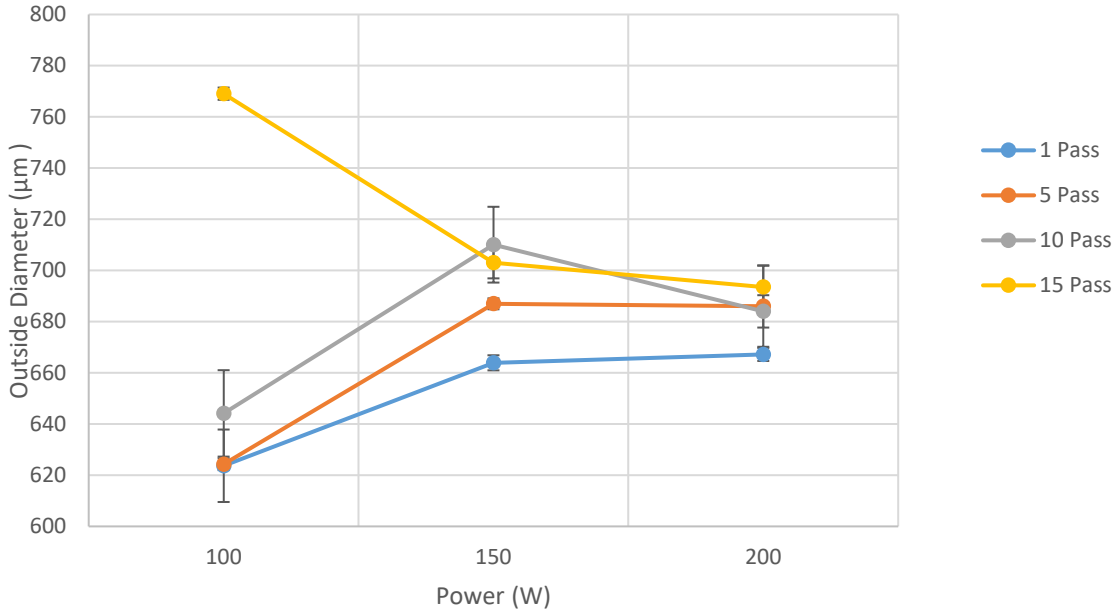

Figure A6. Circles – 0.50 mm OD vs Power

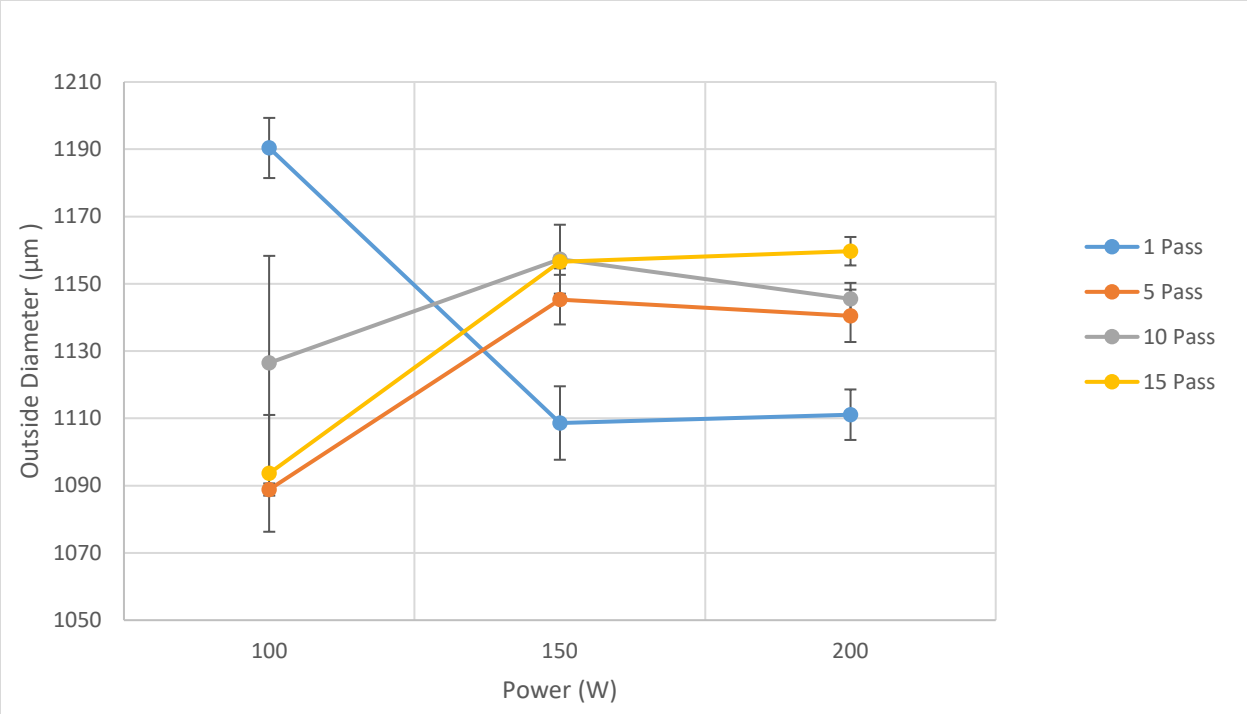

Figure A7. Circles - 1.0 mm OD vs Power

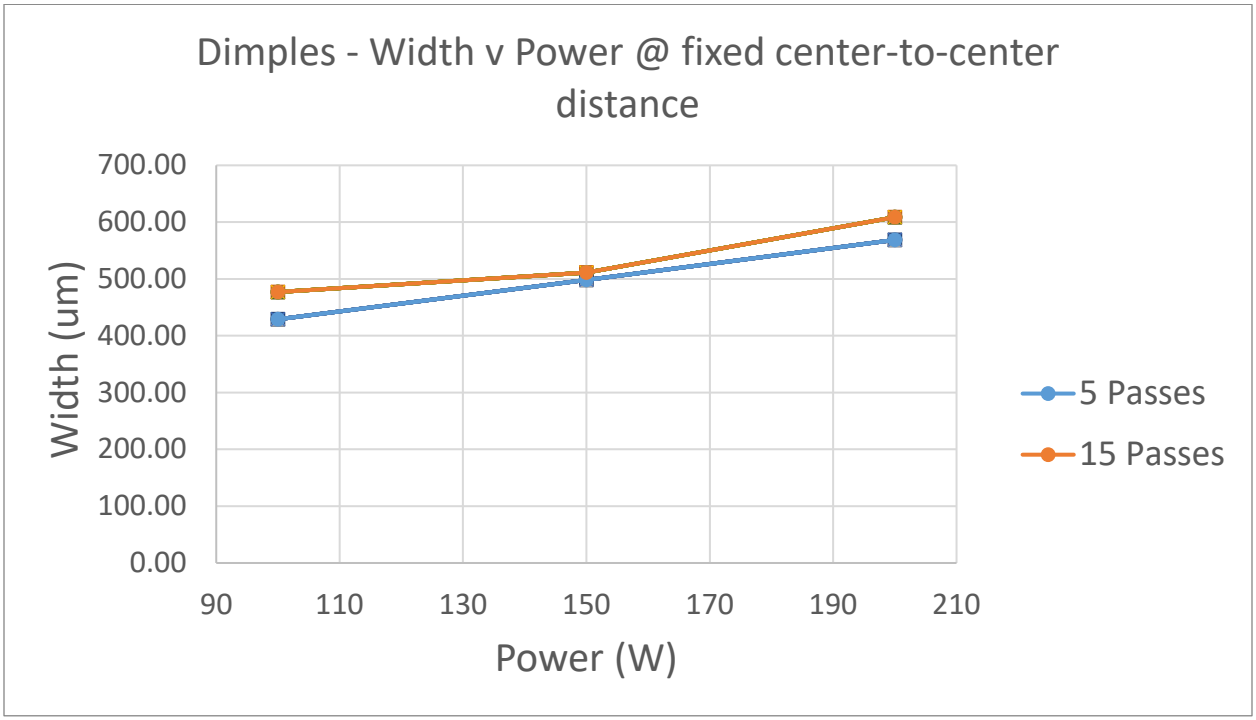

Figure A8. Dimples – Width v Power at Fixed Center-to-Center Distance

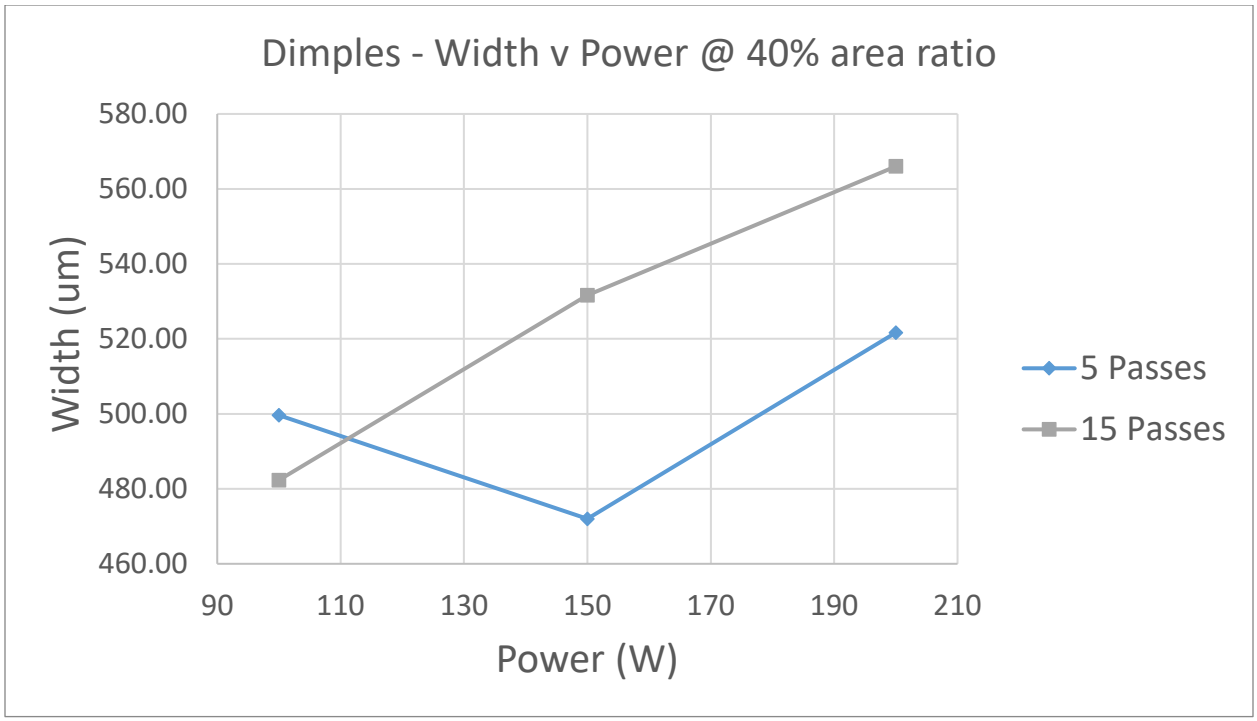

Figure A9. Dimples – Width v Power at 40% Area Ratio

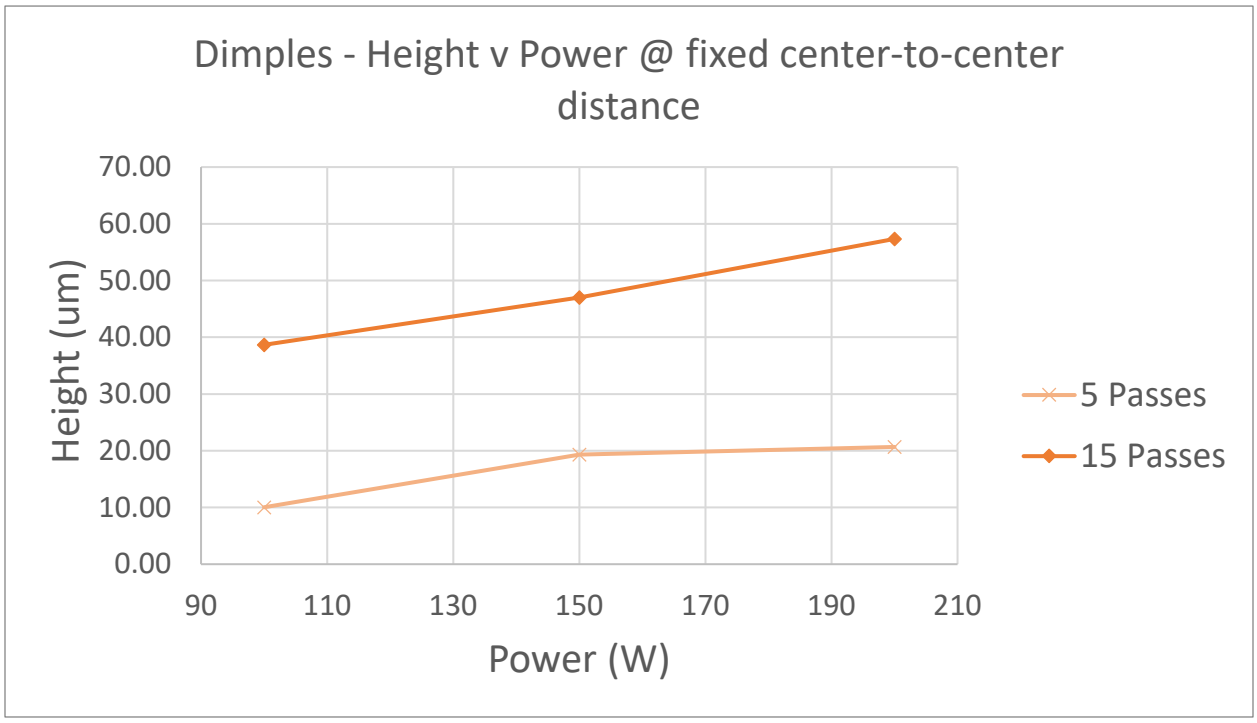

Figure A10. Dimples – Height v Power at Fixed Center-to-Center Distance

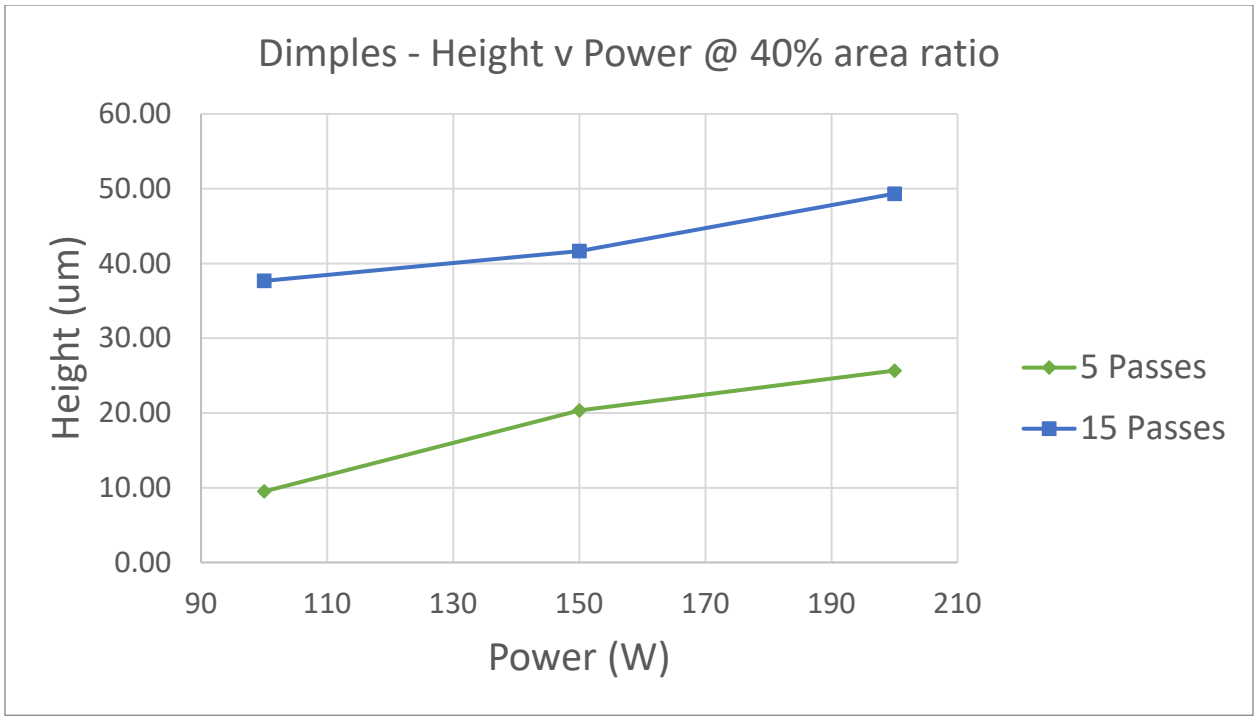

Figure A11. Dimples – Height v Power at 40% Area Ratio

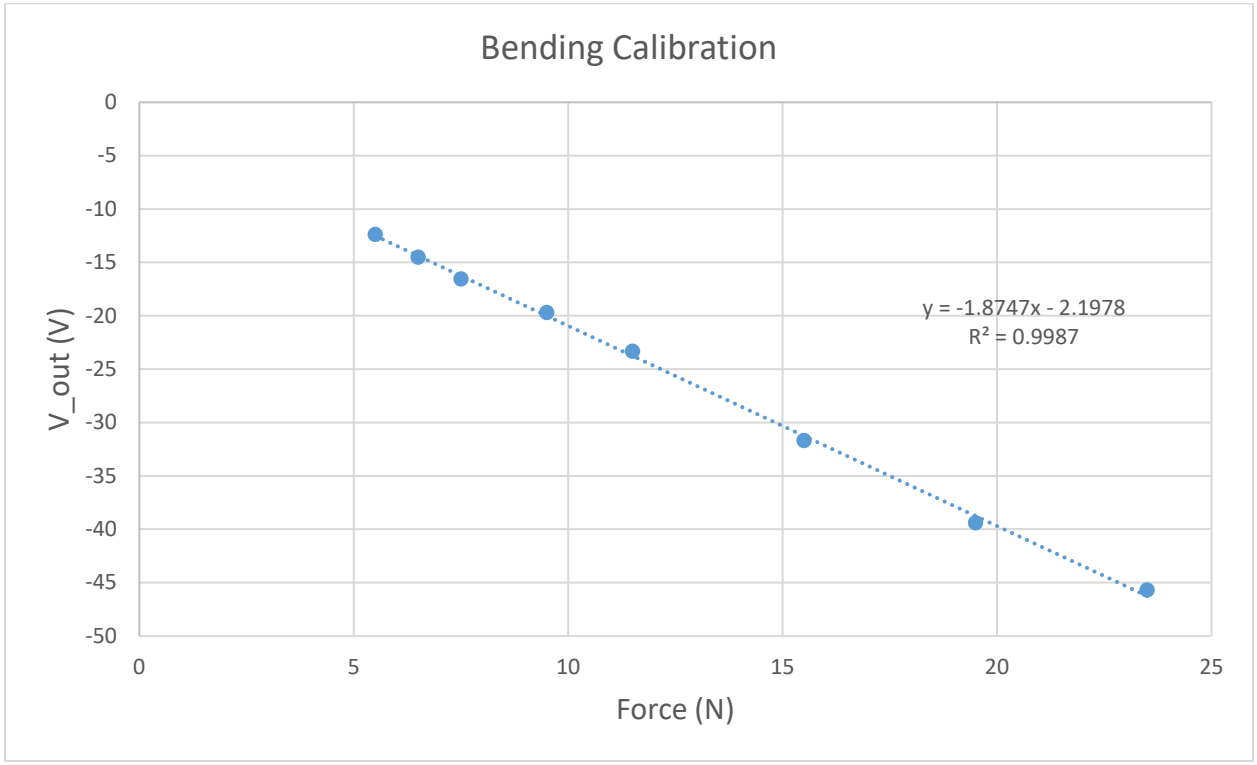

Figure A12. Bending Calibration Curve

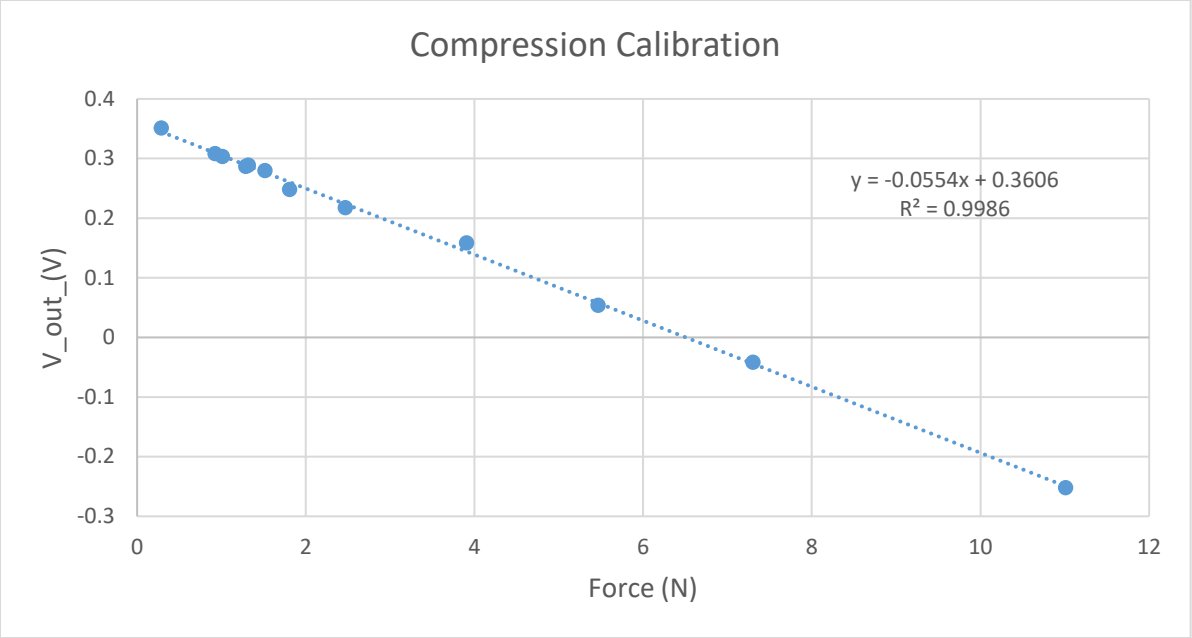

Figure A13. Compression Calibration Curve

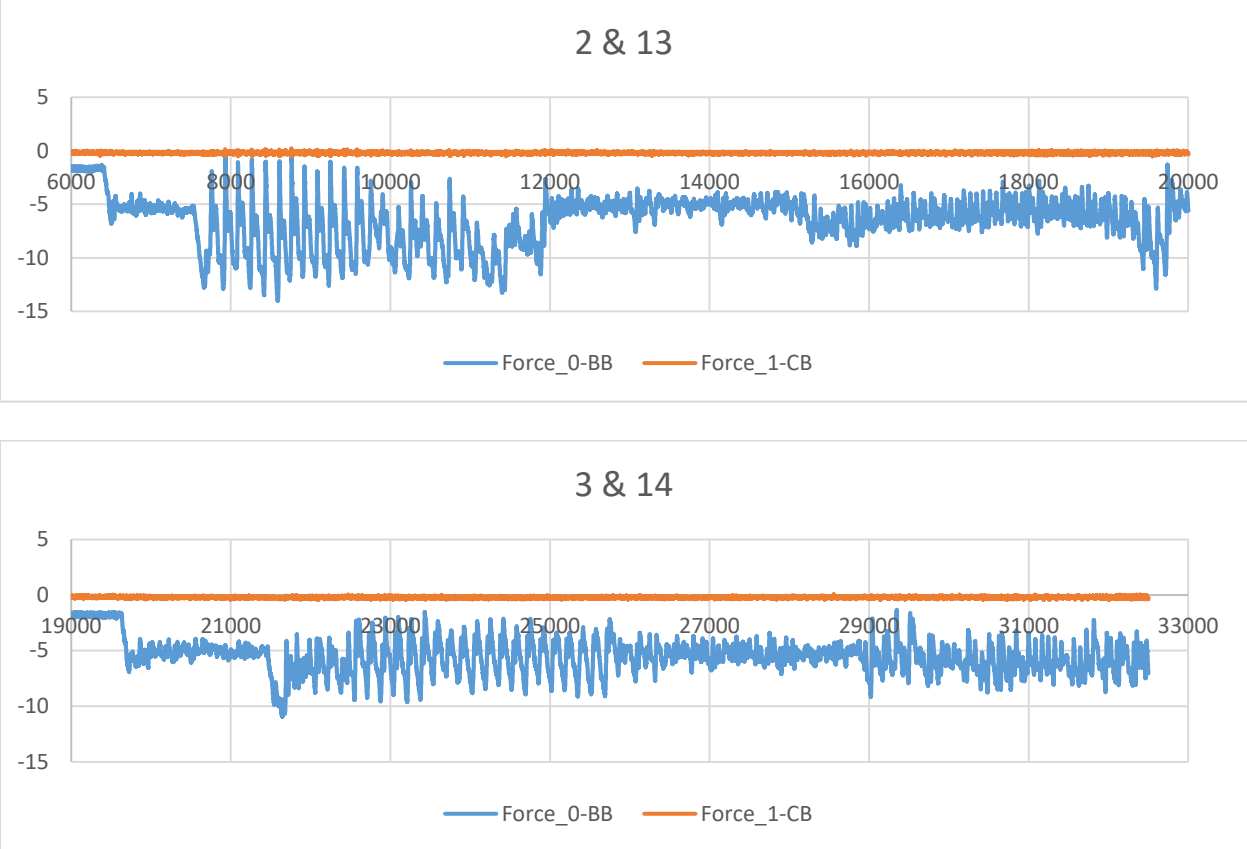

Figure A14. Raw Plots of Output Voltage v Time by Texture Number

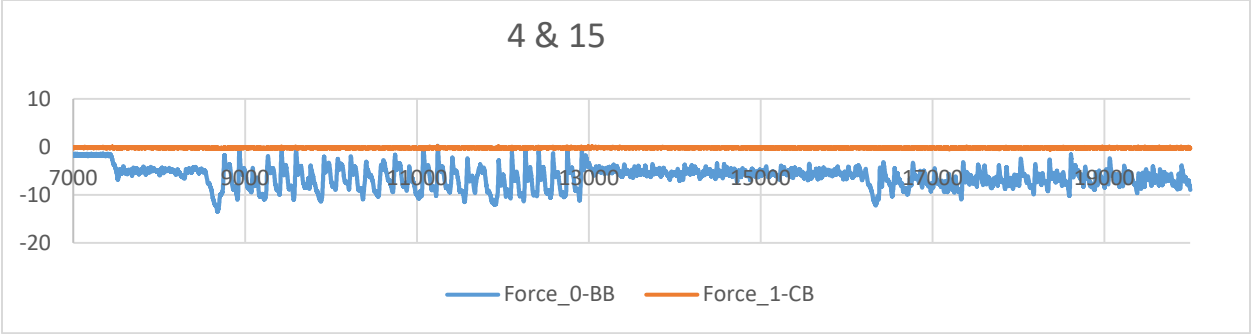

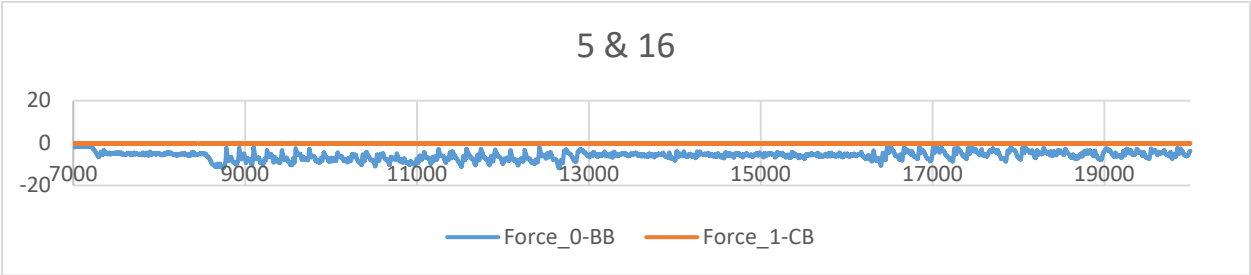

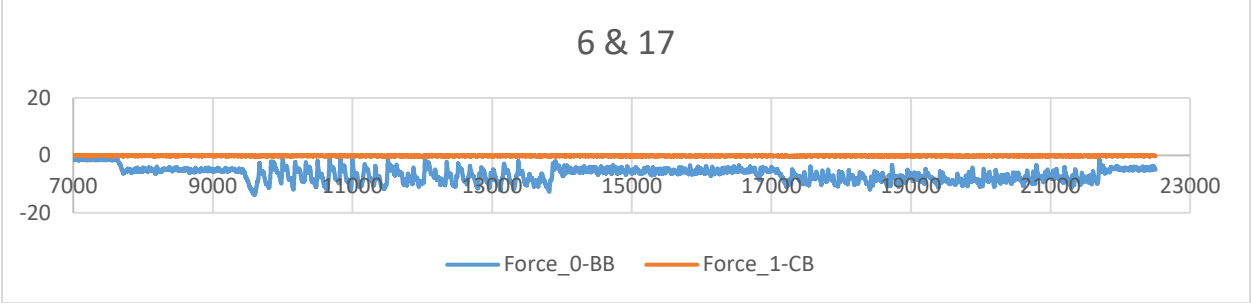

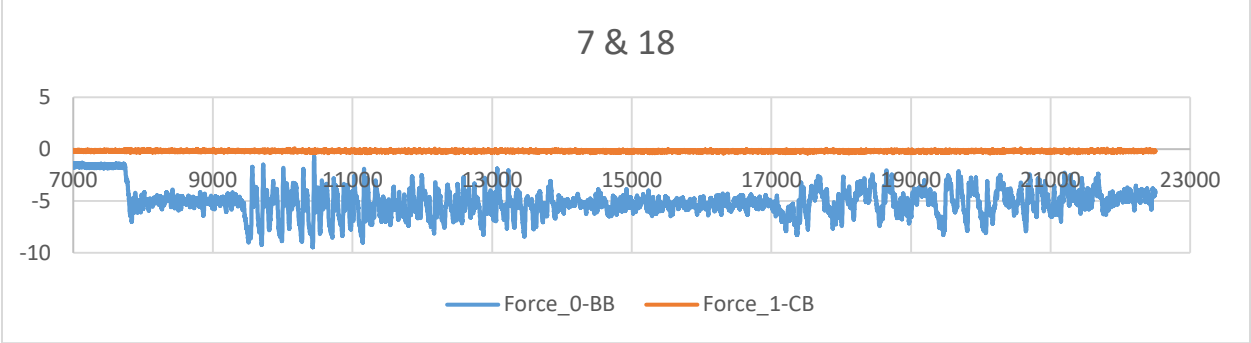

Figure A14. Continued

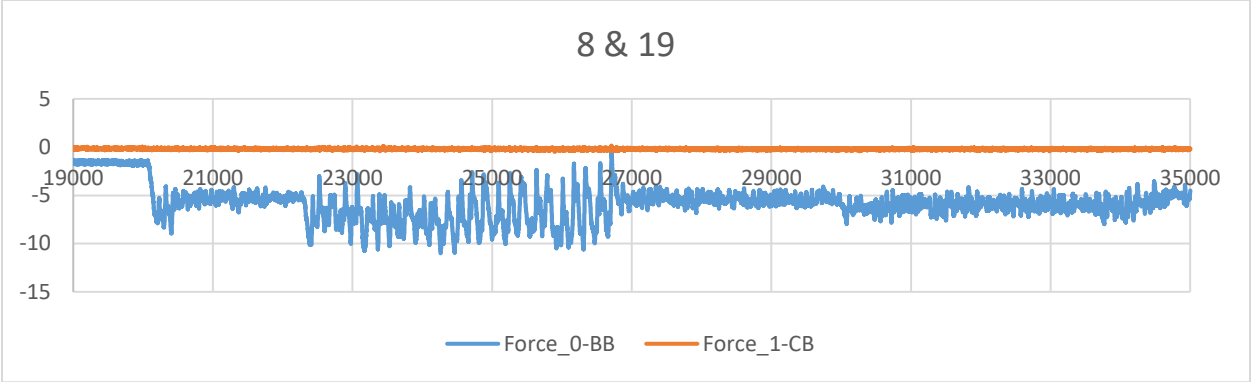

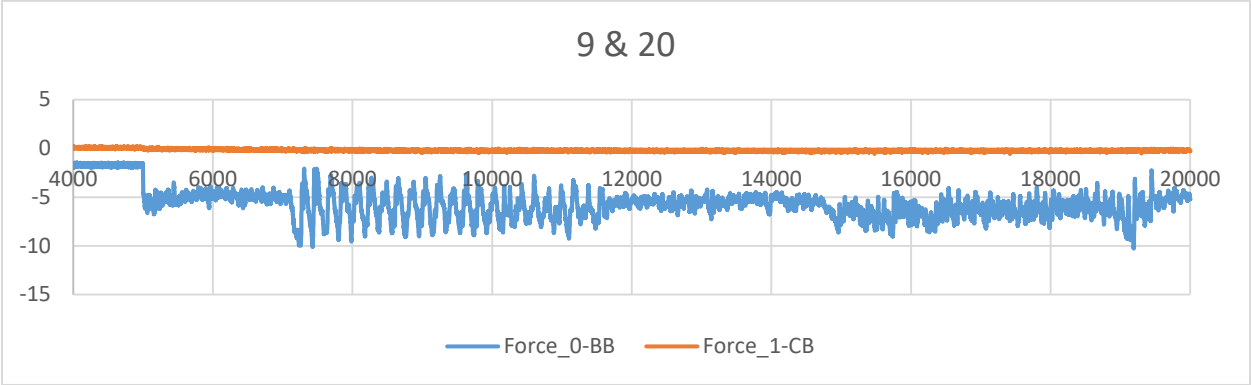

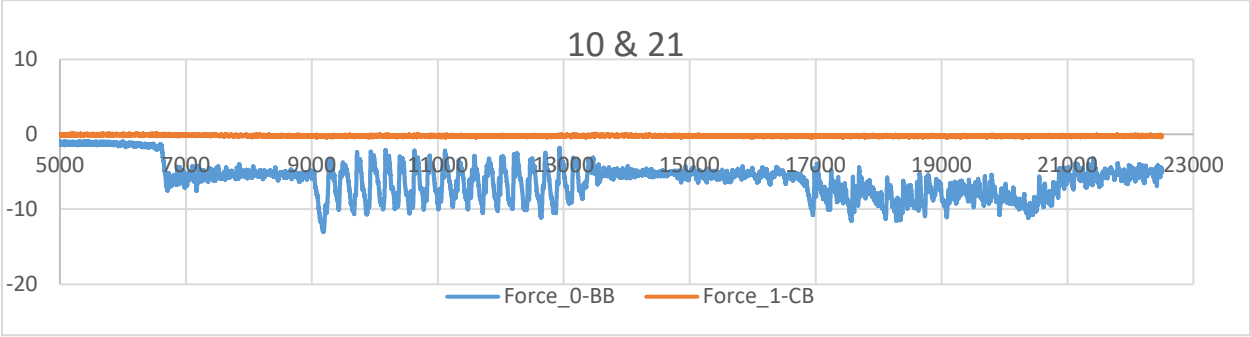

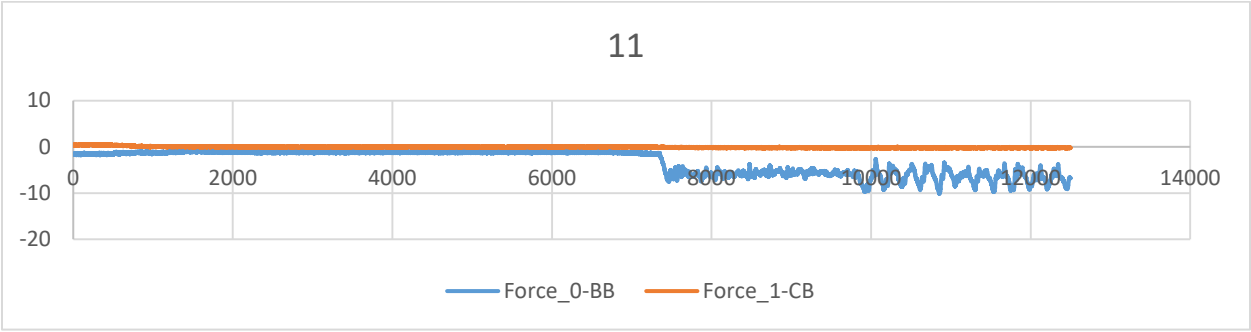

Figure A14. Continued

APPENDIX B

Table B1. Dimples Measurements

Power (W)	# of Passes	avg width		avg depth		set avg width	set avg depth
100	1	-		-		-	-
100	1	-		-			
100	1	-		-			
100	5	260.91		#DIV/0!		275.7	-
100	5	283.69		#DIV/0!			
100	5	282.43		#DIV/0!			
100	10	348.67		32.67		335.8	39.7
100	10	329.33		43.57			
100	10	329.33		43.00			
100	15	348.67		41.67		341.0	36.9
100	15	332.67		36.00			
100	15	341.67		33.00			
150	1	315.67		16.67		284.6	8.2
150	1	278.33		7.00			
150	1	259.67		0.83			
150	5	400.33		14.33		358.6	19.1
150	5	337.67		30.00			
150	5	337.67		13.00			
150	10	368.67		44.67		391.6	44.0
150	10	395.33		42.00			
150	10	410.67		45.33			
150	15	412.67		47.00		417.7	46.1
150	15	430.00		47.67			
150	15	410.33		43.67			
200	1	356.67		17.50		361.1	18.7
200	1	375.33		29.50			
200	1	351.33		9.00			
200	5	429.33		41.17		412.4	35.6
200	5	402.67		30.00			
200	5	405.33		35.67			

Table B1. Continued

Power (W)	# of Passes	avg width		avg depth		set avg width	set avg depth
200	10	421.67		92.00		420.8	80.0
200	10	407.00		87.33			
200	10	433.67		60.67			
200	15	454.67		114.33		445.6	106.2
200	15	397.00		116.33			
200	15	485.00		88.00			

Table B2. Lines Measurements

Power (W)	# of Passes	avg width		avg depth		set avg width	set avg depth
100	1	124.00		3.67			
100	1	123.00		4.27			
100	1	118.67		4.00		121.89	3.98
100	5	140.67		10.17			
100	5	138.67		9.50			
100	5	131.33		10.50		136.89	10.06
100	10	149.67		18.67			
100	10	153.33		17.33			
100	10	152.33		13.00		151.78	16.33
100	15	154.67		24.00			
100	15	155.00		23.00			
100	15	166.67		18.67		158.78	21.89
150	1	133.33		4.17			
150	1	152.67		5.67			
150	1	137.00		6.00		141.00	5.28
150	5	179.67		17.87			
150	5	178.67		15.00			
150	5	176.00		15.67		178.11	16.18
150	10	214.00		33.00			
150	10	202.33		24.17			
150	10	208.33		35.00		208.22	30.72
150	15	197.00		24.50			
150	15	206.33		34.67		198.56	33.00

Table B2. Continued

Power (W)	# of Passes	avg width		avg depth		set avg width	set avg depth
150	15	192.33		39.83		198.56	33.00
200	1	156.67		7.00		154.22	6.67
200	1	148.33		6.33			
200	1	157.67		6.67			
200	5	180.33		11.67		183.11	14.33
200	5	187.67		15.00			
200	5	181.33		16.33			
200	10	158.00		26.83		176.33	26.17
200	10	186.33		26.50			
200	10	184.67		25.17			
200	15	209.33		35.33		200.56	36.89
200	15	199.33		36.33			
200	15	193.00		39.00			